Vascular Smooth Muscle Cell Plasticity and Autophagy in Dissecting Aortic Aneurysms

Clément et al., Smooth muscle cell plasticity in aortic dissection

Marc Clément, PhD; Joel Chappell, PhD; Juliette Raffort, MD; Fabien Lareyre, MD; Marie Vandestienne, MSc; Annabel L Taylor, MRes; Alison Finigan, BS; James Harrison, BS; Martin R Bennett, MD, PhD; Patrick Bruneval, MD; Soraya Taleb, PhD; Helle F Jørgensen, PhD; Ziad Mallat, MD, PhD

From the Division of Cardiovascular Medicine, University of Cambridge, Cambridge, UK (M.C., J.C., J.R., F.L., A.L.T., A.F., J.H., M.R.B., H.F.J., Z.M.), and Institut National de la Santé et de la Recherche Médicale, Universite Paris-Descartes, Paris Cardiovascular Research Center, and Université Paris-Descartes, Paris, France (M.V., P.B., S.T., Z.M.); Department of Vascular Surgery (F.L.) and Clinical Chemistry Laboratory (J.R.), University Hospital of Nice, and Université Côte d'Azur, Nice, France.

M.C. and J.C. contributed equally to this work.

H.F.J. and Z.M. contributed equally to this work.

Correspondence to:

Helle F Jørgensen, PhD, at Division of Cardiovascular Medicine, University of Cambridge, Addenbrooke's Hospital, Cambridge, CB2 2QQ, UK. Tel: +44 1223 762581; E-Mail: hfj22@cam.ac.uk

And Ziad Mallat, MD, PhD, at Division of Cardiovascular Medicine, University of Cambridge, Addenbrooke's Hospital, Cambridge, CB2 2QQ, UK. Tel: +44 1223 768678; E-Mail: zm255@medchl.cam.ac.uk.

Total word count: 5950.

Figures: 7

Subject codes: Pathophysiology; Aneurysm; Smooth muscle cell.

ABSTRACT

Objective— Recent studies suggested the occurrence of phenotypic switching of vascular smooth muscle cells (VSMCs) during the development of aortic aneurysm (AA). However, lineage-tracing studies are still lacking and the behavior of VSMCs during the formation of dissecting AA is poorly understood.

Approach and Results— We used multicolor lineage tracing of VSMCs to track their fate after injury in murine models of angiotensin II-induced dissecting AA. We also addressed the direct impact autophagy on the response of VSMCs to AA dissection. Finally, we studied the relevance of these processes to human AAs. Here, we show that a subset of medial VSMCs undergoes clonal expansion and that VSMC outgrowths are observed in the adventitia and the borders of the false channel during angiotensin II-induced development of dissecting AA. The clonally expanded VSMCs undergo phenotypic switching with downregulation of VSMC differentiation markers and upregulation of phagocytic markers, indicative of functional changes. In particular, autophagy and endoplasmic reticulum (ER) stress responses are activated in the injured VSMCs. Loss of autophagy in VSMCs through deletion of autophagy protein 5 gene (*Atg5*) increases the susceptibility of VSMCs to death, enhances ER stress activation, and promotes inositol-requiring enzyme (IRE)1α-dependent VSMC inflammation. These alterations culminate in increased severity of aortic disease and higher incidence of fatal AA dissection in mice with VSMC-restricted deletion of *Atg5*. We also report increased expression of autophagy and ER stress markers in VSMCs of human dissecting AAs.

Conclusions— VSMCs undergo clonal expansion and phenotypic switching in angiotensin II-induced dissecting aortic aneurysms in mice. We also identify a critical

role for autophagy in regulating VSMC death and ER stress-dependent inflammation with important consequences for aortic wall homeostasis and repair.

Abbreviations:

AA: aortic aneurysm

Ang: angiotensin

Apoe: apolipoprotein e

ATG5: autophagy protein 5

ATG16L1: autophagy protein 16 like 1

ER: endoplasmic reticulum

IRE: inositol-requiring enzyme

LAMP2: Lysosomal Associated Membrane Protein 2

LC3: microtubule-associated protein 1 light chain 3

SMA: smooth muscle actin

TGF: transforming growth factor

VSMC: vascular smooth muscle cell

INTRODUCTION

The response of vascular smooth muscle cells (VSMCs) to injury is a major determinant of the development and progression of vascular diseases, including atherosclerosis, restenosis, and aneurysm [1-3]. In response to injury and inflammation, VSMCs undergo phenotypic switching from a quiescent contractile phenotype to a proliferative, migratory, and synthetic phenotype, and can acquire molecular and cellular features of mesenchymal stem cells and macrophages [4]. VSMC plasticity is well-documented during atherosclerosis and neointima formation, and has been confirmed using lineage-tracing experiments [5-8]. More recently, using multicolor lineage labeling, we demonstrated that VSMC accumulation in atherosclerotic plaques and injury-induced neointimal lesions results from extensive proliferation of a small subset of differentiated but highly plastic medial VSMCs, a variable proportion of which undergo phenotypic switching to phagocyte-like cells [9]. VSMCs also play important roles in the pathophysiology of aortic aneurysm (AA), and recent studies suggested a role for some aspects of VSMC phenotypic switching in AA [10, 11]. However, the plasticity of VSMCs during AA formation has not been assessed. Here we used multicolor lineage labeling of VSMCs to characterize the behavior of VSMCs during the development and progression of angiotensin II (AngII)-induced dissecting AA. We report the occurrence of clonal expansion of a subset of VSMCs in the media, which can outgrow into the adventitia (including the false-channel's borders) of the dissecting AA. The expanded VSMCs undergo phenotypic switching to phagocyte-like cells, and can upregulate autophagy and endoplasmic reticulum (ER) stress markers. Importantly, loss of autophagy in VSMCs promotes VSMC death and ER stress-dependent VSMC inflammation, and aggravates the aortic disease.

METHODS

Data disclosure statement

The data that support the findings of this study are available from the corresponding authors.

Animals

All experiments were performed according to Home Office, UK regulations and approved by the local ethics committee. For lineage tracing, *Myh11-CreERt2/ROSA26-Confetti* males were subjected to 10 intraperitoneal injections of 1 mg tamoxifen over 2 weeks followed by at least 1 week washout. *Tagln*$^{Cre+}$/*Atg5*$^{flox/flox}$ animals were used to assess the role of autophagy in VSMC. Infusion of 1µg/min/Kg AngII, with or without treatment with 10mg/Kg anti-transforming growth factor (TGF)β (clone 1.D.11, BioXCell) was used to induce dissecting AA. Animals were analyzed as described in the Online Data Supplement.

Statistical analysis

Values are shown as average ± SEM. Differences between groups were evaluated using Mann-Whitney test (2 groups), Kruskal-Wallis test followed by uncorrected Dunn's test (> 2 groups), 2-way ANOVA (cell proliferation/survival) or Chi2 test (distribution between 2 groups), as indicated in figure legends. Results were considered statistically significant at $P<0.05$.

RESULTS

Characterization of VSMCs during aortic dissection induced by AngII

VSMCs downregulate contractile gene expression during AA formation [10, 11]. However, the plasticity of VSMCs during AA formation has not been fully characterized. To this end, we used a prototypical model of dissecting AA induced by

AngII, with or without TGFβ inhibition [12, 13]. We first stained for αSMA on cross-sections of mice with aortic dissections. We observed accumulation of αSMA^+ cells in the false channel in 5 out of 5 animals displaying aortic dissection in this experiment. These αSMA^+ cells seemed to expand from the media **(Figure 1A)**, and accumulated in hemorrhagic/thrombotic areas in contact with iron (Perl's staining, **Figure 1B)**, and red blood cells, which may explain their acquisition of heme oxygenase (HMOX)1 expression **(Figure 1C)**. αSMA^+ cells detected in the thrombotic/hemorrhagic region also showed increased expression of the phagocytic marker CD68 **(Figure 1D)** and the lysosomal marker LAMP2 **(Figure 1E),** suggesting that some VSMCs switched towards phagocyte-like cells. We further confirmed our results using flow cytometry analysis of aortic cells isolated from *Apoe*$^{-/-}$ mice infused with AngII for 21 days (**Figure 2**). The proportion of VSMCs ($\alpha SMA^{high}CD90^-$) with high expression of αSMA markedly decreased in dissected aortas compared to controls, whereas a substantial proportion of $\alpha SMA^{int}CD90^{high}$ (myofibroblasts) and $\alpha SMA^{low}CD90^{high}$ (fibroblasts) **(Figure 2A)** were observed in diseased aortas. VSMCs, myofibroblasts and fibroblasts acquired phagocytic markers LAMP2 (**Figure 2B**) and CD68 (**Figure 2C-D**) proportionally to the severity of aortic disease, and cells from dissecting aneurysms were positive for Ter-119, suggesting an association with red blood cells (**Figure 2F-G**). These results suggest that a substantial proportion of VSMCs, myofibroblasts and fibroblasts adopt a phagocyte-like phenotype in dissecting AA.

VSMC clonal expansion and phenotypic switching in dissecting AA

In order to test whether the αSMA^+ cells that have accumulated in the adventitia have originated from pre-existing VSMCs, we used multicolor lineage tracing in *Myh11*-CreERt2/Rosa26-Confetti mice to track VSMCs and their progeny [9]. VSMCs were

labeled by tamoxifen injections before the induction of AA by AngII infusion and TGFβ inhibition **(Figure 3)**. Stochastic labeling of VSMCs using this method results in a mosaic pattern in the non-injured aortic media [9]. We found that αSMA$^+$ cells that accumulated in the adventitia and the false channel in mice with aortic dissection were also positive for Confetti fluorescent reporters (5 out of 6 mice) indicating that they were VSMC derived-cells coming from the media **(Figure 3A)**. Interestingly, in contrast to the stochastic mosaic labeling of the normal aortic media, VSMC-derived cells in the adventitia displayed a non-random color distribution **(Figure 3A)**. We observed large regions containing lineage-labelled cells of a single color or intermixed single colors in all (5/5) animals with VSMC-derived Confetti$^+$ cells outside the medial layer, suggesting that these cell outgrowths are derived from clonal expansion of a small number of cells **(Figure 3A)**. We also found monochromatic patches of VSMCs in the medial layer of 5 out of the 6 animals analyzed **(**>5 cells per patch, **Figure 3B and Figure I in the online-only Data Supplement),** suggesting that proliferation is activated in a subset of medial VSMCs. The clonally expanded VSMCs observed in the adventitial outgrowths and in medial monochromatic patches significantly downregulated their αSMA expression **(Figure 3A and 3B and Figure II in the online-only Data Supplement)**, further supporting that these cells undergo phenotypic switching. To examine whether the accumulation of VSMC-derived cells in the dissected area was a result of TGFβ inhibition, we lineage-traced VSMCs in apolipoprotein e (*Apoe*)$^{-/-}$ animals that develop dissecting AA after AngII treatment in the absence of TGFβ inhibition. The occurrence and extent of monochromatic patches was not affected by TGFβ neutralization in AngII-treated animals (8/15 *Apoe*$^{-/-}$ without anti-TGFβ and 6/10 *Apoe*$^{-/-}$ with anti-TGFβ) (**Figure 3C**). Confetti-positive cells were observed in the thrombotic/hemorrhagic area of 3/6 *Apoe*$^{-/-}$ animals

displaying limited aortic dissection **(Figure III in the online-only Data Supplement)**. Analysis of EdU incorporation **(Figure 3D)** confirmed that VSMCs were proliferating both in the media **(Figure 3E)** and in the adventitial outgrowth areas of dissected aortas **(Figure 3F and Figure IV in the online-only Data Supplement)**. Confetti$^+$ cells in the media expressed almost no phagocytic markers, but the Confetti$^+$ cells that have expanded into the adventitia, started to express HMOX1, CD68 and LAMP2 **(Figure 3G)**. CD90 expression was undetectable in Confetti$^+$ cells, except for a few cells with very low expression (data not shown). Our data indicate that clonal proliferation and phenotypic switching of medial VSMCs are important features of AngII-induced aortic dissection.

Atg5 deficiency in VSMCs promotes the development of severe aortic dissection

The lysosomal pathway, and particularly LAMP2, controls autophagosome maturation [14]. Moreover, autophagy plays critical roles in VSMC biology [15] and has recently been linked with VSMC phenotypic switching [16]. Defective autophagy in VSMC is associated with accelerated VSMC senescence, neointima formation and atherogenesis [15, 17], but its role in the pathophysiology of dissecting AA is still uncertain [18]. Studying aortic cross sections, we found increased expression of autophagy-related protein 16 like 1 (ATG16L1) in medial and adventitial αSMA$^+$ cells of dissecting AA (5 out of 5) compared to very limited staining in VSMCs of healthy aortas **(Figure 4A)**, suggesting a potential role of autophagy in this disease condition. We confirmed that ATG16L1 is expressed in VSMC-derived cells, using the Confetti lineage tracing animals (**Figure VA in the online-only Data Supplement**). ATG5 is essential for all types of autophagy, and we found that ATG5

was also expressed in VSMC-derived Confetti+ cells (**Figure VB and VC in the online-only Data Supplement**). Furthermore, *Atg5* gene expression was upregulated in primary VSMCs at passage 4 in culture compared to *ex vivo* primary VSMCs (**Figure VD in the online-only Data Supplement),** further supporting a potential role of autophagy in phenotypically switched VSMCs. Using $Tagln^{Cre+}/Atg5^{flox/flox}$ mice **(Figure VIA in the online-only Data Supplement)**, we investigated the impact of defective autophagy in VSMCs on the incidence of aortic dissection in mice. There was no difference in the blood pressure response to AngII between $Tagln^{Cre+}/Atg5^{flox/flox}$ and $Tagln^{Cre-}/Atg5^{flox/flox}$ mice **(Figure VIB in the online-only Data Supplement)**. Over 28 days, mice with *Atg5* deficiency in VSMCs showed reduced survival compared with their WT littermates **(Figure 4B)**. 9 out of 17 $Tagln^{Cre+}/Atg5^{flox/flox}$ mice died from aortic rupture compared to 2 out of 14 $Tagln^{Cre-}/Atg5^{flox/flox}$ mice (**Figure 4C and 4D**). Moreover, 3 out of 17 $Tagln^{Cre+}/Atg5^{flox/flox}$ mice died without evidence of aortic rupture at autopsy, but instead presented with hemorrhage in the peritoneum, spleen and intestine, suggesting vascular impairment in those organs. Analysis of aortic tissue samples showed that vascular injury induced by AngII + anti-TGFβ was significantly more severe in mice with VSMC-restricted *Atg5* deletion **(Figure 4D)**, with higher levels of iron deposition (blue Perl's staining) in the media and adventitia **(Figure 4E-F)** as compared to their littermate controls. Thus, defective autophagy in VSMCs increases the incidence and severity of aortic dissection.

***Atg5* deficiency in VSMCs impedes autophagosome formation and enhances cell death**

To confirm that *Atg5* deficiency inhibits autophagy in VSMCs, we analyzed the expression of microtubule-associated protein 1 light chain 3 (LC3) in αSMA$^+$ cells after the induction of AA. Punctate LC3 staining, associated with autophagosome formation, was significantly reduced in *Tagln*$^{Cre+}$/*Atg5*$^{flox/flox}$ mice compared to *Tagln*$^{Cre-}$/*Atg5*$^{flox/flox}$ control animals **(Figure 5A)**. Conversely, *Atg5* deficiency in VSMCs led to a significant accumulation of the autophagosome cargo protein Sqstm1/p62 **(Figure 5B)** as well as LAMP2 **(Figure 5C)**. Loss of *Atg5* was associated with an increase of apoptotic VSMCs in the media, as shown by active CASPASE-3 staining **(Figure 5D)** suggesting that autophagy promotes cell survival. This was confirmed using *in vitro* experiments, which revealed a substantial reduction of VSMC survival (**Figure 5E**) and proliferation (**Figure 5F**) in response to serum, and an increased susceptibility to ER stress-induced cell death (**Figure 5G**) in the absence of *Atg5*.

Atg5 deficiency in VSMCs promotes an ER stress response and IRE1α-dependent inflammation

There is a close interplay between autophagy and the ER stress response, and recent studies indicate that autophagy may resolve ER stress responses through direct removal of IRE1α [19]. Consistent with the latter finding, we observed a substantial accumulation of the ER stress sensor IRE1α in *Atg5*-deficient VSMCs *in vivo* (**Figure 6A**). *In vitro* cultured *Atg5*-deficient VSMCs also showed substantial accumulation of IRE1α in the absence of any external stimulus **(Figure 6B)**. VSMCs respond to IL1 stimulation by abundant secretion of inflammatory cytokines [20] and chemokines [21]. Interestingly, IL1β-induced expression of IL6 **(Figure 6C)**, CXCL1 and CCL2 (**Figure VII in the online-only Data Supplement**) was significantly higher

in *Atg5*-deficient VSMCs compared to WT control cells and was abrogated by inhibition of IRE1α kinase activity. Consistent with the increased inflammatory response, aortic sections of *Tagln*$^{Cre+}$/*Atg5*$^{flox/flox}$ mice treated with AngII + anti-TGFβ showed increased neutrophil accumulation compared to *Tagln*$^{Cre-}$/*Atg5*$^{flox/flox}$ control mice (**Figure 6D**). We also found a tendency (P=0.06) towards increased circulating levels of IL-6 in *Tagln*$^{Cre+}$/*Atg5*$^{flox/flox}$ compared to *Tagln*$^{Cre-}$/*Atg5*$^{flox/flox}$ mice; however, other tested circulating cytokines and chemokines were not different between the 2 groups (**Figure VII in the online-only Data Supplement**). These results indicate that autophagy-dependent regulation of ER stress modulates VSMC and local aortic inflammation.

Autophagy and ER stress are features of human aortic dissection

To examine the relevance of our findings to human pathology, we analyzed sections of human aortas with or without dissection, collected from separate patients. We found that 4 out of 5 samples with aortic dissection contained αSMA$^+$ and TAGLN$^+$ cells **(Figure 7A)** in areas devoid of elastic lamellae outside the media, whereas such features could not be detected in non-dissected normal aortas (n=5) (**Figure VIII in the online-only Data Supplement**). The vast majority of adventitial αSMA$^+$ cells did not express CD90 (**Figure IX in the online-only Data Supplement**) indicating that they were not of fibroblast origin, and suggesting that they have most likely expanded from the aortic media. Although LC3 expression in VSMCs was similar between non-dissected and dissected aortas (Figure 7B), the latter showed increased accumulation of the autophagosome cargo protein SQSTM1/p62 **(Figure 7C)**, and increased expression of the ER stress marker GRP78/Bip **(Figure 7D)**. Our data

suggest that VSMCs of dissected AAs in humans may have deregulated autophagy resulting in ER stress activation.

DISCUSSION

Previous work on the role of VSMCs in AA has focused on the detrimental effects of VSMC death in promoting adverse arterial wall remodeling due to reported medial thinning, degeneration and extensive apoptosis of VSMCs in very late stages of AA development [22, 23]. Notably however, despite medial thinning and VSMC death, ascending thoracic AAs show an increase in overall medial area and have preserved VSMC density, suggesting a hyperplastic response [24, 25]. Animal models of AA also suggest that VSMCs display some aspects of phenotypic switching early during the development of both thoracic and abdominal AA [10, 11]. Here, we have tested the hypothesis that a hyperplastic VSMC response could compensate for increased VSMC death during AA development. Using lineage tracing of pre-existing VSMCs in mice, we found that in response to AngII infusion, a subset of VSMCs clonally expand in the media of the thoracic and abdominal aorta, and in the context of aortic dissection, expand through the aortic wall into the adventitia and the newly formed false channel. We propose that the resulting VSMC-derived cells might play a reparative role at several disease stages, from aneurysm development to aneurysm dissection. Interestingly, large foci of VSMCs also accumulate in areas of extensive elastin degradation corresponding to the external medial layers and adjacent adventitia of human thoracic AAs, suggesting similar pathophysiological mechanisms in human AAs.

Our lineage-tracing experiments demonstrate that a subset of pre-existing VSMCs proliferate, downregulate contractile protein expression and upregulate proteins

associated with a phagocytic-like phenotype in AA. This resembles the VSMC behavior observed in other vascular disease models [6-9], suggesting that the extensive plasticity is an inherent physiologically relevant feature of VSMCs. Importantly, we found many examples of clonal proliferation resulting in monochromatic patches within the medial layer in animals showing no signs of aortic dissection. This observation suggests that activation of proliferation occurs in a larger proportion of VSMCs than what was estimated from the clonal VSMC contribution to neointima formation after vascular injury [9].

The finding that VSMCs downregulate the contractile phenotype in AA is consistent with and further validates previous work [10, 11, 26]. Two recent studies reported that interference with molecular pathways involved in VSMC phenotypic switching may have detrimental effects in AA. VSMC-restricted deletion of KLF4, which has previously been identified as a regulator of several aspects of VSMC phenotypic switching in atherosclerosis [7], reduced aortic disease severity in mouse models of AA [26], although it did not abrogate the disease. A more recent study identified a role for HDAC9-MALAT1-BRG1 complex in the downregulation of the contractile VSMC phenotype in AAs driven by mutations of the TGFβ pathway; VSMC-restricted deletion of MALAT1 significantly preserved the contractile phenotype of VSMCs and reduced AA development in a mouse mode of Marfan with *Fbn1* mutation [11]. These studies are consistent with a detrimental role of the downregulation of the contractile phenotype of VSMCs in AAs. However, KLF4 and MALAT1 may impact other VSMC functions beyond, and maybe independently, of their role in regulating the contractile phenotype of VSMCs.

Beyond the downregulation of differentiation and contractile markers of VSMCs, VSMC phenotypic switching induces a wide range of functions, which might have

opposing functions on AA formation and progression. Here, we assessed the particular role of VSMC autophagy in AA, and found that loss of *Atg5* in VSMC reduced autophagosome generation and resulted in increased disease progression and mortality in AngII-treated animals with TGFβ inhibition. Previously, the role of VSMC autophagy in the development of AA was examined in $Atg7^{flox/flox}/Tagln^{Cre/+}$ mice [18]. The authors concluded that mice with smooth muscle cell-specific *Atg7* deficiency do not develop dissecting abdominal AA in response to AngII [18]. Importantly, that study was conducted using AngII infusion under normo-cholesterolemic conditions where mice are resistant to AA [12, 13]. Additional cues, such as the presence of hypercholesterolemia [12] or the concomitant blockade of TGFβ signaling pathway [13, 27], are required to promote the susceptibility of the aorta to aneurysm formation and dissection in response to AngII infusion. In our present study, the use of a previously validated model of dissecting AA [13, 27] revealed a clear detrimental effect of defective autophagy in VSMCs on AA development. The incidence and severity of dissected AAs were significantly higher in mice with *Atg5* deletion in VSMCs. Of note, 18% of the mice (25% of the mice that died suddenly) showed evidence of extra-aortic hemorrhage in the peritoneum, spleen and intestine, suggesting that defective autophagy in VSMCs may be associated with widespread impairment of the vascular response to injury. Taken together, the data show that autophagy in VSMCs is critically required for the maintenance of vascular integrity during the development and progression of AAs. This vasculo-protective effect may be explained at least in part, by the role of autophagy in preserving VSMC survival in response to injury. Our data also identify a role of autophagy in the regulation of VSMC inflammation, potentially through the degradation of IRE1α [19]. IRE1α has previously been involved in mediating inflammatory responses downstream of toll-like

receptors [28, 29] and C-type lectin receptors [30] but its role in IL1R1 signaling pathways has not been addressed. We speculate that this inter-connection between autophagy, ER stress responses and inflammatory pathways is of major importance to the outcome of the reparative process after injury, and merits further consideration. Finally, the direct impact of autophagy on the regulation of VSMC clonal proliferation and phenotypic switching will need to be addressed. It will also be interesting to address the direct impact of autophagy deletion on the response of VSMC to AngII stimulation.

CONCLUSIONS

We provide genetic evidence for the activation of VSMC proliferation, selective clonal expansion and phenotypic switching towards phagocytic-like phenotypes in VSMCs during the development of dissecting AA. We identify a critical role for autophagy in the preservation of vessel integrity, possibly through limitation of VSMC death and ER stress-dependent inflammation. The results advance our understanding of the reparative mechanisms that operate during aneurysm development and progression, which could be exploited clinically. Future studies to identify the precise stimuli responsible for VSMC proliferation and accumulation in this context are important to reveal potential new therapeutic targets.

ACKNOWLEDGMENTS

The authors would like to thank the Wellcome Trust - Medical Research Council, Institute of Metabolic Science, Metabolic Research Laboratories, Imaging core, Wellcome Trust Strategic Award (100574/Z/12/Z) and the Cambridge National Institute for Health Research Biomedical Research Centre Cell Phenotyping Hub.

SOURCES OF FUNDING

Z.M. is supported by the British Heart Foundation, UK. The project also received funding from INSERM, France. J.C. and A.T. are supported by British Heart Foundation (BHF) studentships (RE/13/6/30180, FS/14/59/31282). H.F.J. is supported by the BHF Cambridge Centre for Research Excellence (RE/13/6/30180) and the BHF Oxbridge Centre for Regenerative Medicine (RM/13/3/30158, RM/17/2/33380).

DISCLOSURES

None.

REFERENCES

1. Alexander MR, Owens GK. Epigenetic control of smooth muscle cell differentiation and phenotypic switching in vascular development and disease. *Annu Rev Physiol*. 2012;74:13-40.

2. Tellides G, Pober JS. Inflammatory and immune responses in the arterial media. *Circ Res*. 2015;116:312-322.

3. Bennett MR, Sinha S, Owens GK. Vascular Smooth Muscle Cells in Atherosclerosis. *Circ Res*. 2016;118:692-702.

4. Gomez D, Swiatlowska P, Owens GK. Epigenetic Control of Smooth Muscle Cell Identity and Lineage Memory. *Arterioscler Thromb Vasc Biol*. 2015;35:2508-2516.

5. Herring BP, Hoggatt AM, Burlak C, Offermanns S. Previously differentiated medial vascular smooth muscle cells contribute to neointima formation following vascular injury. *Vasc Cell*. 2014;6:21.

6. Feil S, Fehrenbacher B, Lukowski R, Essmann F, Schulze-Osthoff K, Schaller M, Feil R. Transdifferentiation of vascular smooth muscle cells to macrophage-like cells during atherogenesis. *Circ Res*. 2014;115:662-667.

7. Shankman LS, Gomez D, Cherepanova OA, Salmon M, Alencar GF, Haskins RM, Swiatlowska P, Newman AA, Greene ES, Straub AC, Isakson B, Randolph GJ, Owens GK. KLF4-dependent phenotypic modulation of smooth muscle cells has a key role in atherosclerotic plaque pathogenesis. *Nat Med*. 2015;21:628-637.

8. Cherepanova OA, Gomez D, Shankman LS, et al. Activation of the pluripotency factor OCT4 in smooth muscle cells is atheroprotective. *Nat Med*. 2016;22:657-665.

9. Chappell J, Harman JL, Narasimhan VM, Yu H, Foote K, Simons BD, Bennett MR, Jorgensen HF. Extensive Proliferation of a Subset of Differentiated, yet Plastic, Medial Vascular Smooth Muscle Cells Contributes to Neointimal Formation in Mouse Injury and Atherosclerosis Models. *Circ Res*. 2016;119:1313-1323.

10. Ailawadi G, Moehle CW, Pei H, Walton SP, Yang Z, Kron IL, Lau CL, Owens GK. Smooth muscle phenotypic modulation is an early event in aortic aneurysms. *J Thorac Cardiovasc Surg*. 2009;138:1392-1399.

11. Lino Cardenas CL, Kessinger CW, Cheng Y, et al. An HDAC9-MALAT1-BRG1 complex mediates smooth muscle dysfunction in thoracic aortic aneurysm. *Nat Commun*. 2018;9:1009.

12. Daugherty A, Manning MW, Cassis LA. Angiotensin II promotes atherosclerotic lesions and aneurysms in apolipoprotein E-deficient mice. *J Clin Invest*. 2000;105:1605-1612.

13. Wang Y, Ait-Oufella H, Herbin O, Bonnin P, Ramkhelawon B, Taleb S, Huang J, Offenstadt G, Combadiere C, Renia L, Johnson JL, Tharaux PL, Tedgui A, Mallat Z. TGF-beta activity protects against inflammatory aortic aneurysm progression and complications in angiotensin II-infused mice. *J Clin Invest*. 2010;120:422-432.

14. Saftig P, Beertsen W, Eskelinen EL. LAMP-2: a control step for phagosome and autophagosome maturation. *Autophagy*. 2008;4:510-512.

15. De Meyer GR, Grootaert MO, Michiels CF, Kurdi A, Schrijvers DM, Martinet W. Autophagy in vascular disease. *Circ Res*. 2015;116:468-479.

16. Song TF, Huang LW, Yuan Y, Wang HQ, He HP, Ma WJ, Huo LH, Zhou H, Wang N, Zhang TC. LncRNA MALAT1 regulates smooth muscle cell phenotype switch via activation of autophagy. *Oncotarget*. 2018;9:4411-4426.

17. Grootaert MO, da Costa Martins PA, Bitsch N, Pintelon I, De Meyer GR, Martinet W, Schrijvers DM. Defective autophagy in vascular smooth muscle cells accelerates senescence and promotes neointima formation and atherogenesis. *Autophagy*. 2015;11:2014-2032.

18. Ramadan A, Singh KK, Quan A, Plant PJ, Al-Omran M, Teoh H, Verma S. Loss of vascular smooth muscle cell autophagy exacerbates angiotensin II-associated aortic remodeling. *J Vasc Surg*. 2017.

19. Tschurtschenthaler M, Adolph TE, Ashcroft JW, et al. Defective ATG16L1-mediated removal of IRE1alpha drives Crohn's disease-like ileitis. *J Exp Med*. 2017;214:401-422.

20. Loppnow H, Libby P. Proliferating or interleukin 1-activated human vascular smooth muscle cells secrete copious interleukin 6. *J Clin Invest*. 1990;85:731-738.

21. Alexander MR, Murgai M, Moehle CW, Owens GK. Interleukin-1beta modulates smooth muscle cell phenotype to a distinct inflammatory state relative to PDGF-DD via NF-kappaB-dependent mechanisms. *Physiol Genomics*. 2012;44:417-429.

22. Lopez-Candales A, Holmes DR, Liao S, Scott MJ, Wickline SA, Thompson RW. Decreased vascular smooth muscle cell density in medial degeneration of human abdominal aortic aneurysms. *Am J Pathol*. 1997;150:993-1007.

23. Henderson EL, Geng YJ, Sukhova GK, Whittemore AD, Knox J, Libby P. Death of smooth muscle cells and expression of mediators of apoptosis by T lymphocytes in human abdominal aortic aneurysms. *Circulation*. 1999;99:96-104.

24. Lesauskaite V, Tanganelli P, Sassi C, Neri E, Diciolla F, Ivanoviene L, Epistolato MC, Lalinga AV, Alessandrini C, Spina D. Smooth muscle cells of the media in the dilatative pathology of ascending thoracic aorta: morphology,

immunoreactivity for osteopontin, matrix metalloproteinases, and their inhibitors. *Hum Pathol*. 2001;32:1003-1011.

25. Tang PC, Coady MA, Lovoulos C, Dardik A, Aslan M, Elefteriades JA, Tellides G. Hyperplastic cellular remodeling of the media in ascending thoracic aortic aneurysms. *Circulation*. 2005;112:1098-1105.

26. Salmon M, Johnston WF, Woo A, Pope NH, Su G, Upchurch GR, Jr., Owens GK, Ailawadi G. KLF4 regulates abdominal aortic aneurysm morphology and deletion attenuates aneurysm formation. *Circulation*. 2013;128:S163-174.

27. Chen X, Rateri DL, Howatt DA, Balakrishnan A, Moorleghen JJ, Cassis LA, Daugherty A. TGF-beta Neutralization Enhances AngII-Induced Aortic Rupture and Aneurysm in Both Thoracic and Abdominal Regions. *PLoS One*. 2016;11:e0153811.

28. Qiu Q, Zheng Z, Chang L, et al. Toll-like receptor-mediated IRE1alpha activation as a therapeutic target for inflammatory arthritis. *EMBO J*. 2013;32:2477-2490.

29. Bettigole SE, Glimcher LH. Endoplasmic reticulum stress in immunity. *Annu Rev Immunol*. 2015;33:107-138.

30. Clement M, Basatemur G, Masters L, Baker L, Bruneval P, Iwawaki T, Kneilling M, Yamasaki S, Goodall J, Mallat Z. Necrotic Cell Sensor Clec4e Promotes a Proatherogenic Macrophage Phenotype Through Activation of the Unfolded Protein Response. *Circulation*. 2016;134:1039-1051.

Highlights

- Vascular smooth muscle cells (VSMCs) of the aortic media undergo clonal expansion in mouse models of dissecting aortic aneurysms.
- The clonally expanded VSMCs undergo phenotypic switching towards phagocytic-like phenotypes.
- Autophagy and endoplasmic reticulum (ER) stress responses are activated in some VSMCs. Autophagy in VSMCs control inositol-requiring enzyme (IRE)1α-dependent VSMC inflammation.
- We identify a critical role for autophagy in preserving vessel integrity and reducing the occurrence and severity of aortic dissection, possibly through limitation of VSMC death and ER stress-dependent inflammation.
- Our results suggest that promotion of proliferation and autophagy in VSMCs while inhibiting IRE1α-dependent inflammation may promote aortic wall repair and limit the development of dissecting aortic aneurysm.

Figure Legends

Figure 1. αSMA$^+$ cells accumulate outside of the media and express phagocytic makers after aortic dissection.

A-C – Representative images of anti-αSMA staining on cross sections of abdominal aortas from mice treated with AngII and anti-TGFβ for 10 days showing αSMA$^+$ cell outgrowths from the medial layer (A, right panel), as compared to sections from control mice (A, left panel). On consecutive sections, Perl's (B) and anti-HMOX1 (C) staining show that αSMA$^+$ cells in an iron rich environment (Perl's$^+$) express the heme catabolic enzyme (HMOX1). D-F – Representative images of cryosections co-stained for αSMA and CD68 (D) or LAMP2 (E) showing that CD68 and LAMP2 colocalize with αSMA$^+$ cells in the adventitial layers of aortic dissection. Hoechst (blue) represents nuclear staining. Images are representative of immunostainings done on 5 mice with aortic dissection.

Figure 2. Vascular smooth muscle cells, fibroblasts and myofibroblasts express phagocytic markers after aortic dissection (AD).

Flow cytometric analysis of stromal cells (CD45$^-$) in the aorta of 5-month-old male *Apoe*$^{-/-}$ mice infused with AngII for 21 days (n=13). Littermate control *Apoe*$^{-/-}$ mice were left untreated (top panel, n=4). A – Left panel: Representative images of aortic samples from untreated or AngII infused *Apoe*$^{-/-}$ mice that either did not (no AD) or did develop an aortic dissection (AD). Enzymatically digested aortas were analysed by flow cytometry. Middle/right panel: Representative dot plots showing the gating strategy used to analyze αSMA^{high}CD90$^-$ cells (VSMCs), αSMA$^-$CD90$^+$ (fibroblast phenotype) and αSMA^{low}CD90$^+$ (myofibroblasts). Aortic dissection induced by AngII (lower panel, n=4 mice) dramatically reduced the percentage of αSMA^{high}CD90$^-$ cells

(VSMCs) within $CD45^-$ cells, but increased the percentages of αSMA^-CD90^+ (fibroblast phenotype) and $\alpha SMA^{low}CD90^+$ (myofibroblasts). B – Quantification of LAMP2 expression by $\alpha SMA^{high}CD90^-$ cells (VSMCs), αSMA^-CD90^+ (fibroblast phenotype) and $\alpha SMA^{low}CD90^+$ (myofibroblasts) and flow chart showing the expression of LAMP2 by $\alpha SMA^{high}CD90^-$ cells (VSMCs). *p<0.05 AngII (AD) vs AngII (no AD) and untreated *Apoe*$^{-/-}$ mice, Kruskal-Wallis test followed by Uncorrected Dunn's test. C – Representative dot plots showing the percentage of $\alpha SMA^{high}CD90^-$ cells (VSMCs) expressing CD68 in untreated $Apoe^{-/-}$ mice (left panel) and AngII treated *Apoe*$^{-/-}$ mice without (middle panel) or with (right panel) aortic dissection (AD). D – Quantification of CD68 expression by aortic $\alpha SMA^{high}CD90^-$ cells (VSMCs), αSMA^-CD90^+ (fibroblast phenotype) and $\alpha SMA^{low}CD90^+$ (myofibroblasts). *p<0.05 AngII (AD) vs AngII (no AD) and untreated *Apoe*$^{-/-}$ mice, Kruskal-Wallis test followed by Uncorrected Dunn's test. E – Representative dot plots showing the percentage of αSMA^-CD90^+ (fibroblast phenotype) and $\alpha SMA^{low}CD90^+$ (myofibroblasts) expressing CD68 in dissected aortas. F – Representative dot plots showing the percentage of Ter-119 positive $\alpha SMA^{high}CD90^-$ cells (VSMCs). G – Quantification of Ter-119 positive $\alpha SMA^{high}CD90^-$ cells (VSMCs), αSMA^-CD90^+ (fibroblast phenotype) and $\alpha SMA^{low}CD90^+$ (myofibroblasts). * p<0.05 AngII (AD) vs AngII (no AD) and untreated *Apoe*$^{-/-}$ mice, Kruskal-Wallis test followed by Uncorrected Dunn's test. H – Representative dot plots showing the percentage of Ter-119 positive $\alpha SMA^{neg}CD90^+$ (fibroblasts) and $\alpha SMA^{int}CD90^+$ (myofibroblasts) in aortas with aortic dissection (AD).

Figure 3. VSMCs undergo clonal proliferation and phenotypic switching upon AngII treatment and aortic dissection.

A, B - Representative confocal images of abdominal aortic cross-sections from *Myh11-CreERt2/Rosa26-Confetti* animals treated with AngII and anti-TGFβ. Signals for confetti colors (blue = CFP, yellow = YFP, red = RFP, green = GFP), immunostaining for anti-αSMA (magenta) and DAPI (white) are shown as indicated. (A) αSMA^+ cells observed in the false channel of *Confetti* animals that developed an aortic dissection express the genetic Confetti lineage label, demonstrating that they are derived from Myh11-expressing VSMCs. Notably, the non-random color distribution of VSMC-derived cells in the adventitia indicates clonal expansion of a small number of cells. (B) Monochromatic patches of VSMC-derived cells in the media express lower levels of αSMA compared to non-expanding medial VSMCs. C - Quantification of clonal expansion in the media, represented as the fraction of monochromatic patches with ≥5 cells/patch, in the aorta of *Myh11-CreERt2/Rosa26-Confetti/Apoe*$^{-/-}$ mice treated with AngII alone or AngII + anti-TGFβ, compared to healthy controls (No AngII). Blocking TGFβ activity did not alter clonal VSMC expansion. 67-318 VSMC patches were analyzed per mouse. No AngII: n=4, AngII: n=14; AngII + anti-TGFβ: n=10. *p<0.05 for No AngII *vs*. AngII and No AngII *vs*. AngII + anti-TGFβ. Data were analyzed using Kruskal-Wallis test followed by Uncorrected Dunn's test. D - Quantification of EdU incorporation in VSMC-derived, Confetti-positive cells in *Myh11-CreERt2/Rosa26-Confetti/Apoe*$^{-/-}$ mice infused with AngII ± anti-TGFβ and injected with EdU from day 14 to day 21 of AngII infusion. AngII: n=13; AngII + anti-TGFβ: n=9. E, F - Representative confocal images of EdU staining in sections from AngII-treated *Myh11-CreERt2/Rosa26-Confetti/Apoe*$^{-/-}$ mice. Clonal expansion of VSMCs in the media (E) and adventitial outgrowth (F) is associated with DNA synthesis (proliferation) after AngII infusion. Arrow heads (colored according to Confetti color) indicate EdU^+ VSMCs. A low magnification

image of panels F and G is available as Figure IV in the online-only Data Supplement**.** G - Representative images showing expression of HMOX1, CD68 and LAMP2 in sections of a dissected aorta from *Myh11-CreERt2/Rosa26-Confetti/Apoe*$^{-/-}$ mice infused with AngII. Images show adventitial regions containing VSMC-derived cells and yellow arrow heads indicate Confetti-positive VSMC-derived cells expressing HMOX1, CD68 or LAMP2. L: Lumen, M: Media, A: adventitia.

Figure 4. ATG5 deletion in VSMCs (*Talgn*$^{Cre+}$/*Atg5*$^{flox/flox}$ mice) increases susceptibility to aortic rupture induced by AngII and anti-TGFβ infusion.

A – Representative images of anti-αSMA and anti-ATG16L1 staining of abdominal aortic cross sections from untreated mice (healthy aorta, n=3) and mice infused with AngII and anti-TGFβ that developed a dissection (n=5). αSMA^{+} cells (in the media and in the adventitial outgrowth) express elevated levels of ATG16L1 compared to healthy controls and the staining shows a punctuate pattern, suggesting that autophagosomes are forming. B-F – *Tagln*$^{Cre-}$ (n=14, black) and *Tagln*$^{Cre+}$ (n=17, white) *Atg5*$^{flox/flox}$ male littermate mice were infused with AngII + anti-TGFβ. B – Survival curves. *p<0.05 *Tagln*$^{Cre-}$ vs *Tagln*$^{Cre+}$, Log-rank (Mantel-Cox) test. C – Representative images of thoraco-abdominal aorta. D – Severity of aortic dissections assessed macroscopically (I-normal appearance; II-thickening of the aortic wall; III-dissection; IV-fatal aortic rupture). *p<0.05 *Tagln*$^{Cre-}$ vs *Tagln*$^{Cre+}$, Chi square test. E-F – Quantification (E) and representative pictures (F) of iron deposition (blue Perl's staining) in the aortic wall (I-no iron deposition; II-mild iron deposition; III- substantial iron accumulation in some cells; IV-high accumulation of iron in numerous cells). *p<0.05 *Tagln*$^{Cre-}$ vs *Tagln*$^{Cre+}$, Chi squared test.

Figure 5. Impaired autophagy in VSMCs impairs autophagosome formation and enhances cell death.

A-D – Aortic cross section from *Tagln*$^{Cre-}$ (n=14, black) and *Tagln*$^{Cre+}$ (n=17, white) *Atg5*$^{flox/flox}$ mice infused with AngII + anti-TGFβ for 28 days were analyzed by confocal microscopy. A – Representative images showing αSMA staining (top panels) and LC3 signal (lower panels). The quantification of autophagosome formation in VSMCs was done using a filter showing background in Cyan, low LC3 staining appears in black and LC3 bright spots in white (Autophagosomes). ***p<0.001 *Tagln*$^{Cre-}$ vs *Tagln*$^{Cre+}$, Mann-Whitney test. B – Representative images showing αSMA (top) and p62 staining (lower panel). Quantification of p62 signal in αSMA-positive VSMCs is shown to the right. ***p<0.001 *Tagln*$^{Cre-}$ vs *Tagln*$^{Cre+}$, Mann-Whitney test. C – Representative images showing LAMP2 and αSMA staining and quantification of lysosome accumulation in VSMCs. **p<0.01 *Tagln*$^{Cre-}$ vs *Tagln*$^{Cre+}$, Mann-Whitney test. D – Representative images showing αSMA and active CASPASE-3 staining. Quantification of the number of active CASPASE-3-positive apoptotic cells in the media is shown on the right. *p<0.05 *Tagln*$^{Cre-}$ vs *Tagln*$^{Cre+}$, Mann-Whitney test. E-F – Primary VSMCs were derived from the aorta of *Tagln*$^{Cre-}$ and *Tagln*$^{Cre+}$ *Atg5*$^{flox/flox}$ mice and cultured for 4-7 passages prior to analysis. Mean ± SEM of technical quadruplicates are shown. E – Serum starved VSMCs were stimulated with serum and cell density analyzed by MTT. *p<0.05, ***p<0.001 *Tagln*$^{Cre-}$ vs *Tagln*$^{Cre+}$ at each time point, 2-way ANOVA followed by uncorrected Fisher's test. F – BrdU incorporation by serum starved VSMCs and cells supplemented with FBS for 48 hours. *p<0.05 *Tagln*$^{Cre-}$ vs *Tagln*$^{Cre+}$ with 10% FBS, Mann-Whitney test. G – VSMCs were incubated with increasing doses of Thapsigargin for 16 hours. Cell density was analyzed using MTT assay and

normalized to untreated *Tagln*$^{Cre-}$ cells. **p<0.01, ***p<0.001 *Tagln*$^{Cre-}$ vs *Tagln*$^{Cre+}$ at each time point, 2-way ANOVA followed by uncorrected Fisher's test.

Figure 6. ATG5 deficiency in VSMCs promotes inflammation via the ER-stress sensor IRE1α.

A – Representative images and quantification of IRE1α immunofluorescence signals in αSMA^{+} cells on aortic cross-sections from *Tagln*$^{Cre-}$ (n=14, black) and *Tagln*$^{Cre+}$ (n=17, white) *Atg5*$^{flox/flox}$ mice infused with AngII and anti-TGFβ for 28 days. **p<0.01 *Tagln*$^{Cre-}$ vs *Tagln*$^{Cre+}$, Mann-Whitney test. B – Representative images of IRE1α immunostaining of primary VSMCs derived from the aorta of *Tagln*$^{Cre-}$ and *Tagln*$^{Cre+}$ *Atg5*$^{flox/flox}$ mice cultured in vitro. C – IL-6 secretion by primary VSMCs derived from the aorta of *Tagln*$^{Cre-}$ and *Tagln*$^{Cre+}$ *Atg5*$^{flox/flox}$ mice stimulated for 16 hours with IL1β (100 pg/ml) in the presence or absence of the IRE1α kinase inhibitor (Apy29, 20μM) in vitro. Mean ± SEM of technical quadruplicates are shown. *p<0.05, ***p<0.001 *Tagln*$^{Cre-}$ vs *Tagln*$^{Cre+}$, 2-way ANOVA followed by uncorrected Fisher's test. D – Representative images and quantification of Ly6G immunostaining on aortic cross-sections from *Tagln*$^{Cre-}$ (n=14) and *Tagln*$^{Cre+}$ (n=17) *Atg5*$^{flox/flox}$ mice infused with AngII + anti-TGFβ for 28 days. *p<0.05 *Tagln*$^{Cre-}$ vs *Tagln*$^{Cre+}$, Mann-Whitney test.

Figure 7. Human aortic dissections are associated with impaired autophagy and ER-stress response in VSMCs.

A-D – Human thoracic aortic samples from non-dissected (n=4-5) and dissected (n=5) aortas were immunostained and analyzed by confocal microscopy. A – Representative images showing that αSMA^{+} and TAGLN^{+} cells are detected outside the media (dotted line depicts the external elastic laminae) in the adventitial layer of

dissected thoracic aorta (4 out of 5 samples) but not in non-dissected samples (0 out of 5 samples). B-D – Representative images and quantification of the expression of LC3 (B), SQSTM1/p62 (C) and GRP78/Bip (D) in αSMA$^+$ cells in the media of non-dissected (n=4-5, white) and dissected aortic samples (n=5, black). *p<0.05 non-dissected vs dissected, Mann-Whitney test.

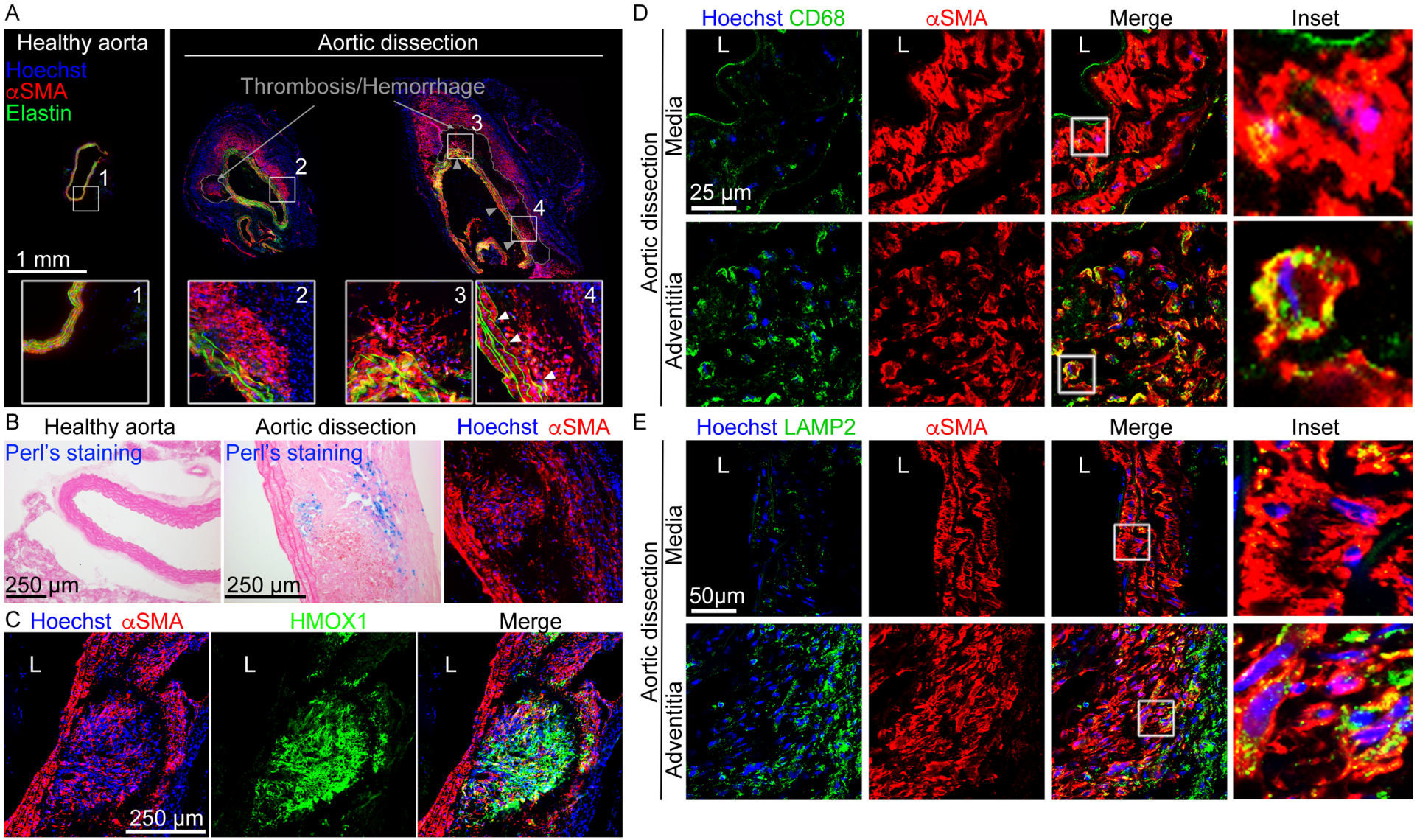
A
Healthy aorta
Hoechst
αSMA
Elastin
1
1 mm
Aortic dissection
Thrombosis/Hemorrhage
2
3
4
B
Healthy aorta
Aortic dissection
Hoechst αSMA
Perl's staining
Perl's staining
250 μm
250 μm
C
Hoechst αSMA
HMOX1
Merge
L
250 μm
D
Hoechst CD68
αSMA
Merge
Inset
Aortic dissection
Media
Adventitia
L
25 μm
E
Hoechst LAMP2
αSMA
Merge
Inset
Aortic dissection
Media
Adventitia
L
50μm

Figure 1

Figure 1. αSMA$^+$ cells accumulate outside of the media and express phagocytic makers after aortic dissection.
A-C – Representative images of anti-αSMA staining on cross sections of abdominal aortas from mice treated with AngII and anti-TGFβ for 10 days showing αSMA$^+$ cell outgrowths from the medial layer (A, right panel), as compared to sections from control mice (A, left panel). On consecutive sections, Perl's (B) and anti-HMOX1 (C) staining show that αSMA$^+$ cells in an iron rich environment (Perl's$^+$) express the heme catabolic enzyme (HMOX1). D-F – Representative images of cryosections co-stained for αSMA and CD68 (D) or LAMP2 (E) showing that CD68 and LAMP2 colocalize with αSMA$^+$ cells in the adventitial layers of aortic dissection. Hoechst (blue) represents nuclear staining. Images are representative of immunostainings done on 5 mice with aortic dissection.

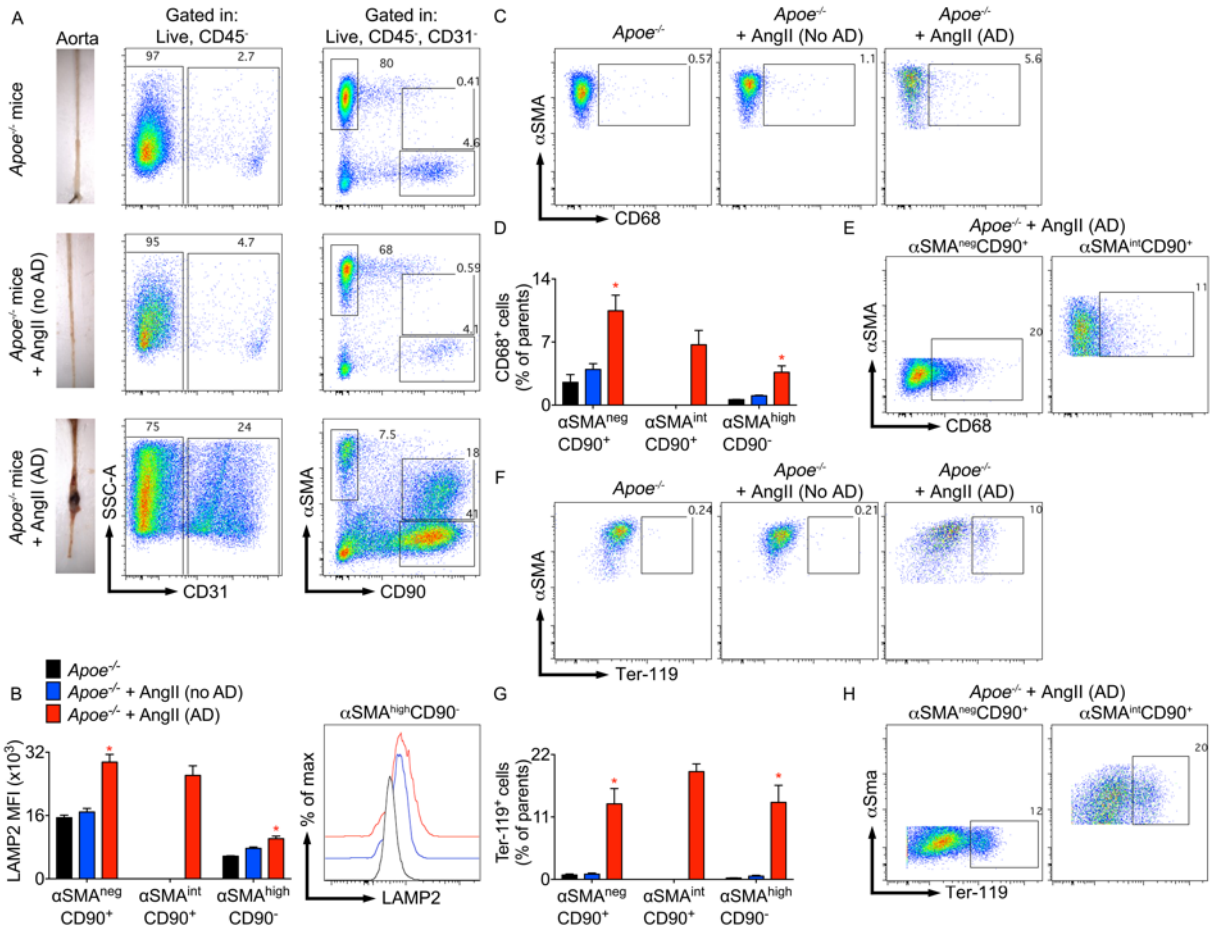

Figure 2. Vascular smooth muscle cells, fibroblasts and myofibroblasts express phagocytic markers after aortic dissection (AD).

Flow cytometric analysis of stromal cells (CD45$^-$) in the aorta of 5-month-old male *Apoe*$^{-/-}$ mice infused with AngII for 21 days (n=13). Littermate control *Apoe*$^{-/-}$ mice were left untreated (top panel, n=4). A – Left panel: Representative images of aortic samples from untreated or AngII infused *Apoe*$^{-/-}$ mice that either did not (no AD) or did develop an aortic dissection (AD). Enzymatically digested aortas were analysed by flow cytometry. Middle/right panel: Representative dot plots showing the gating strategy used to analyze αSMA^{high}CD90$^-$ cells (VSMCs), αSMA$^-$CD90$^+$ (fibroblast phenotype) and αSMA^{low}CD90$^+$ (myofibroblasts). Aortic dissection induced by AngII (lower panel, n=4 mice) dramatically reduced the percentage of αSMA^{high}CD90$^-$ cells (VSMCs) within CD45$^-$ cells, but increased the percentages of αSMA$^-$CD90$^+$ (fibroblast phenotype) and αSMA^{low}CD90$^+$ (myofibroblasts). B – Quantification of LAMP2 expression by αSMA^{high}CD90$^-$ cells (VSMCs), αSMA$^-$CD90$^+$ (fibroblast phenotype) and αSMA^{low}CD90$^+$ (myofibroblasts) and flow chart showing the expression of LAMP2 by αSMA^{high}CD90$^-$ cells (VSMCs). *p<0.05 AngII (AD) vs AngII (no AD) and untreated *Apoe*$^{-/-}$ mice, Kruskal-Wallis test followed by Uncorrected Dunn's test. C – Representative dot plots showing the percentage of αSMA^{high}CD90$^-$ cells (VSMCs) expressing CD68 in untreated Apoe$^{-/-}$ mice (left panel) and AngII treated *Apoe*$^{-/-}$ mice without (middle panel) or with (right panel) aortic dissection (AD). D – Quantification of CD68 expression by aortic αSMA^{high}CD90$^-$ cells (VSMCs), αSMA$^-$CD90$^+$ (fibroblast phenotype) and αSMA^{low}CD90$^+$ (myofibroblasts). *p<0.05 AngII (AD) vs AngII (no AD) and untreated *Apoe*$^{-/-}$ mice, Kruskal-Wallis test followed by Uncorrected Dunn's test. E – Representative dot plots showing the percentage of αSMA$^-$CD90$^+$ (fibroblast phenotype) and αSMA^{low}CD90$^+$ (myofibroblasts) expressing CD68 in dissected aortas. F –

Representative dot plots showing the percentage of Ter-119 positive $\alpha SMA^{high}CD90^{-}$ cells (VSMCs). G – Quantification of Ter-119 positive $\alpha SMA^{high}CD90^{-}$ cells (VSMCs), $\alpha SMA^{-}CD90^{+}$ (fibroblast phenotype) and $\alpha SMA^{low}CD90^{+}$ (myofibroblasts). * $p<0.05$ AngII (AD) vs AngII (no AD) and untreated *Apoe*$^{-/-}$ mice, Kruskal-Wallis test followed by Uncorrected Dunn's test. H – Representative dot plots showing the percentage of Ter-119 positive $\alpha SMA^{neg}CD90^{+}$ (fibroblasts) and $\alpha SMA^{int}CD90^{+}$ (myofibroblasts) in aortas with aortic dissection (AD).

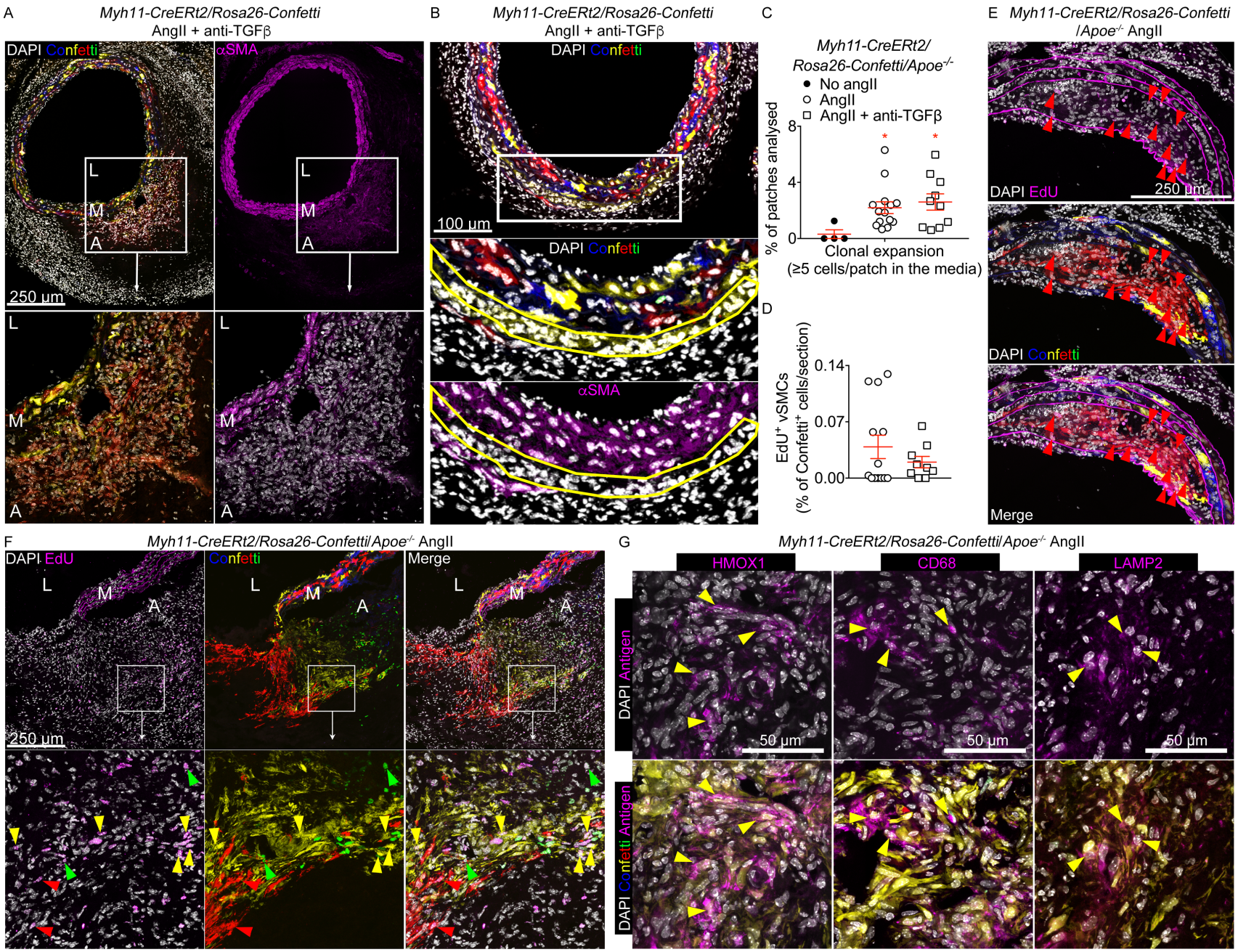
A
Myh11-CreERt2/Rosa26-Confetti
AngII + anti-TGFβ
DAPI Confetti
αSMA
L
M
A
250 μm
B
Myh11-CreERt2/Rosa26-Confetti
AngII + anti-TGFβ
DAPI Confetti
100 μm
αSMA
C
Myh11-CreERt2/
Rosa26-Confetti/Apoe-/-
No angII
AngII
AngII + anti-TGFβ
% of patches analysed
Clonal expansion
(≥5 cells/patch in the media)
D
EdU+ vSMCs
(% of Confetti+ cells/section)
0.14
0.07
0.00
E
Myh11-CreERt2/Rosa26-Confetti
/Apoe-/- AngII
DAPI EdU
250 μm
DAPI Confetti
Merge
F
Myh11-CreERt2/Rosa26-Confetti/Apoe-/- AngII
DAPI EdU
Confetti
Merge
250 μm
G
Myh11-CreERt2/Rosa26-Confetti/Apoe-/- AngII
HMOX1
CD68
LAMP2
DAPI Antigen
DAPI Confetti Antigen
50 μm

Figure 3

Figure 3. VSMCs undergo clonal proliferation and phenotypic switching upon AngII treatment and aortic dissection.

A, B - Representative confocal images of abdominal aortic cross-sections from *Myh11-CreERt2/Rosa26-Confetti* animals treated with AngII and anti-TGFβ. Signals for confetti colors (blue = CFP, yellow = YFP, red = RFP, green = GFP), immunostaining for anti-αSMA (magenta) and DAPI (white) are shown as indicated. (A) αSMA^+ cells observed in the false channel of *Confetti* animals that developed an aortic dissection express the genetic Confetti lineage label, demonstrating that they are derived from Myh11-expressing VSMCs. Notably, the non-random color distribution of VSMC-derived cells in the adventitia indicates clonal expansion of a small number of cells. (B) Monochromatic patches of VSMC-derived cells in the media express lower levels of αSMA compared to non-expanding medial VSMCs.

C - Quantification of clonal expansion in the media, represented as the fraction of monochromatic patches with ≥5 cells/patch, in the aorta of *Myh11-CreERt2/Rosa26-Confetti/Apoe*$^{-/-}$ mice treated with AngII alone or AngII + anti-TGFβ, compared to healthy controls (No angII). Blocking TGFβ activity did not alter clonal VSMC expansion. 67-318 VSMC patches were analyzed per mouse. No angII: n=4, AngII: n=14; AngII + anti-TGFb: n=10. *$p<0.05$ for No angII *vs*. AngII and No angII *vs*. AngII + anti-TGFβ. Data were analysed using Kruskal-Wallis test followed by Uncorrected Dunn's test.

D - Quantification of EdU incorporation in VSMC-derived, Confetti-positive cells in *Myh11-CreERt2/Rosa26-Confetti/Apoe*$^{-/-}$ mice infused with AngII ± anti-TGFβ and injected with EdU from day 14 to day 21 of AngII infusion. AngII: n=13; AngII + anti-TGFβ: n=9.

E, F - Representative confocal images of EdU staining in sections from AngII-treated *Myh11-CreERt2/Rosa26-Confetti/Apoe*$^{-/-}$ mice. Clonal expansion of VSMCs in the media (E) and adventitial outgrowth (F) is associated with DNA synthesis (proliferation) after AngII infusion. Arrow heads (colored according to Confetti color) indicate EdU^+ VSMCs. A low magnification image of panels F and G is available as Figure IV in the online-only Data Supplement**.**

G - Representative images showing expression of HMOX1, CD68 and LAMP2 in sections of a dissected aorta from *Myh11-CreERt2/Rosa26-Confetti/Apoe*$^{-/-}$ mice infused with AngII. Images show adventitial regions containing VSMC-derived cells and yellow arrow heads indicate Confetti-positive VSMC-derived cells expressing HMOX1, CD68 or LAMP2.

L: Lumen, M: Media, A: adventitia.

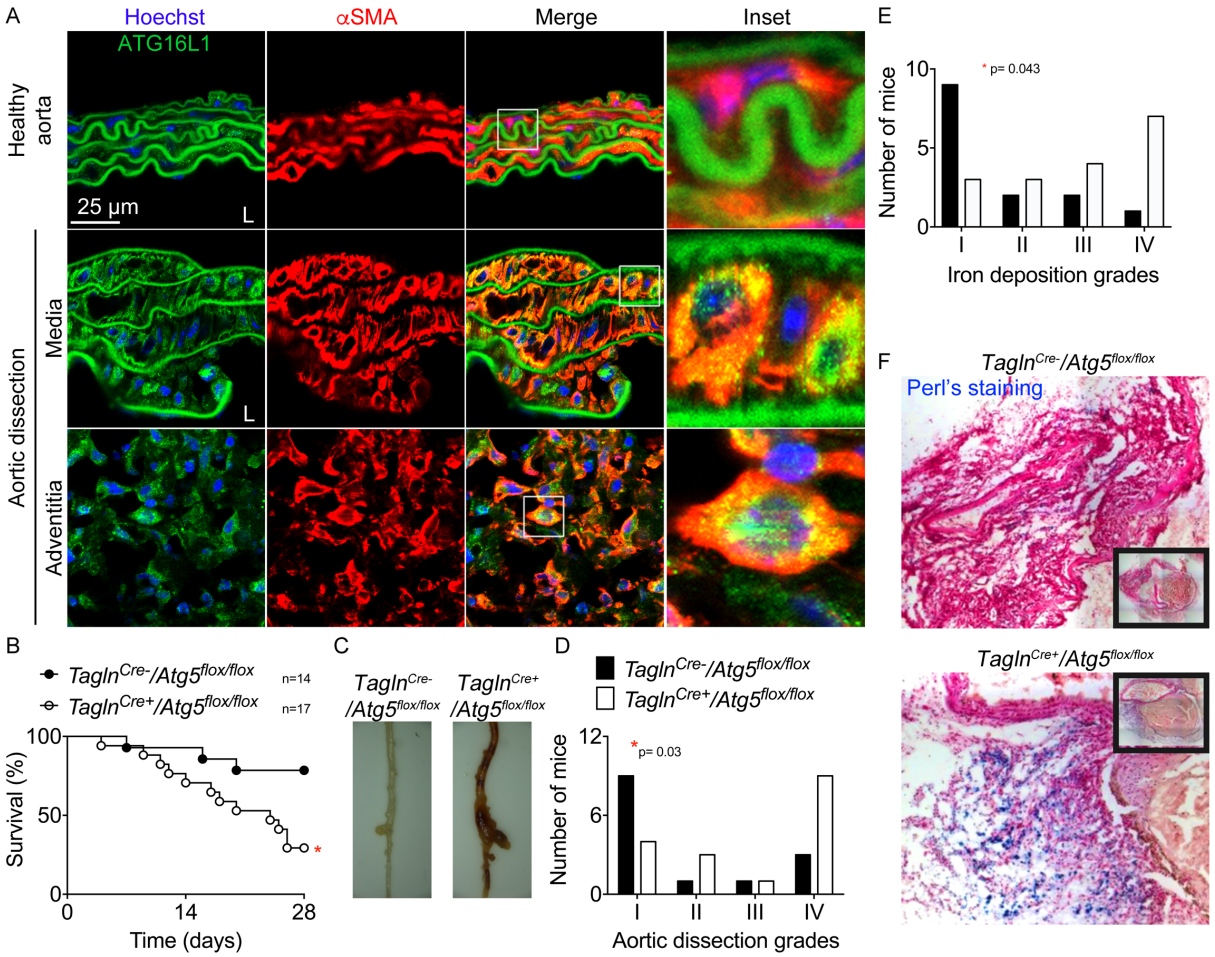

Figure 4. ATG5 deletion in VSMCs (*TaIgn^{Cre+}/Atg5$^{flox/flox}$* mice) increases susceptibility to aortic rupture induced by AngII and anti-TGFβ infusion.

A – Representative images of anti-αSMA and anti-ATG16L1 staining of abdominal aortic cross sections from untreated mice (healthy aorta, n=3) and mice infused with AngII and anti-TGFβ that developed a dissection (n=5). αSMA$^+$ cells (in the media and in the adventitial outgrowth) express elevated levels of ATG16L1 compared to healthy controls and the staining shows a punctuate pattern, suggesting that autophagosomes are forming.

B-F – *Tagln^{Cre-}* (n=14, black) and *Tagln^{Cre+}* (n=17, white) *Atg5$^{flox/flox}$* male littermate mice were infused with AngII + anti-TGFβ. B – Survival curves. *p<0.05 *Tagln^{Cre-}* vs *Tagln^{Cre+}*, Log-rank (Mantel-Cox) test. C – Representative images of thoraco-abdominal aorta. D – Severity of aortic dissections assessed macroscopically (I-normal appearance; II-thickening of the aortic wall; III- dissection; IV-fatal aortic rupture). *p<0.05 *Tagln^{Cre-}* vs *Tagln^{Cre+}*, Chi square test. E-F – Quantification (E) and representative pictures (F) of iron deposition (blue Perl's staining) in the aortic wall (I-no iron deposition; II-mild iron deposition; III- substantial iron accumulation in some cells; IV-high accumulation of iron in numerous cells). *p<0.05 *Tagln^{Cre-}* vs *Tagln^{Cre+}*, Chi squared test.

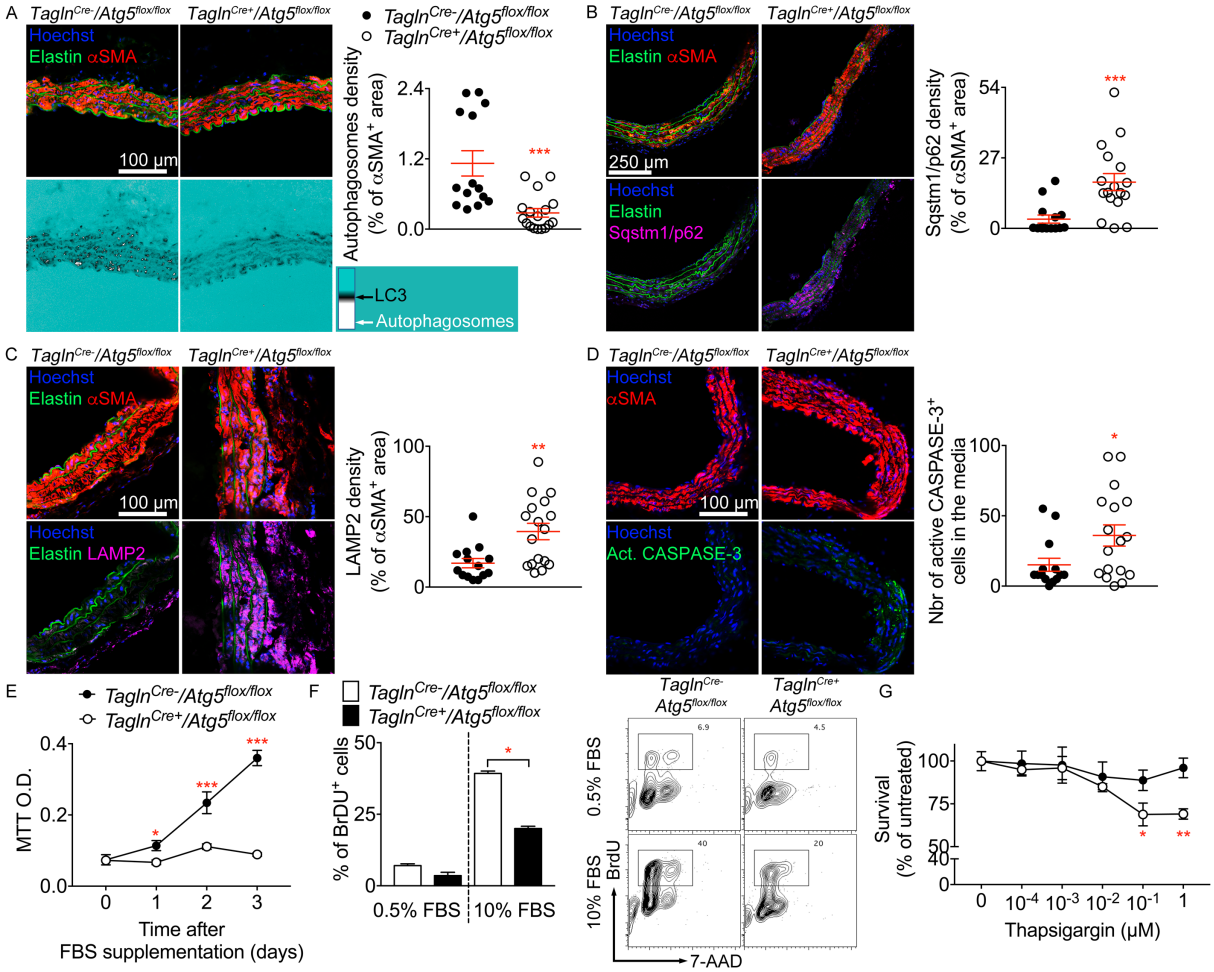

Figure 5. Impaired autophagy in VSMCs impairs autophagosome formation and enhances cell death.

A-D – Aortic cross section from *Tagln*$^{Cre-}$ (n=14, black) and *Tagln*$^{Cre+}$ (n=17, white) *Atg5*$^{flox/flox}$ mice infused with AngII + anti-TGFβ for 28 days were analyzed by confocal microscopy. A – Representative images showing αSMA staining (top panels) and LC3 signal (lower panels). The quantification of autophagosome formation in VSMCs was done using a filter showing background in Cyan, low LC3 staining appears in black and LC3 bright spots in white (Autophagosomes). ***p<0.001 *Tagln*$^{Cre-}$ vs *Tagln*$^{Cre+}$, Mann-Whitney test. B – Representative images showing αSMA (top) and p62 staining (lower panel). Quantification of p62 signal in αSMA-positive VSMCs is shown to the right. ***p<0.001 *Tagln*$^{Cre-}$ vs *Tagln*$^{Cre+}$, Mann-Whitney test. C – Representative images showing LAMP2 and αSMA staining and quantification of lysosome accumulation in VSMCs. **p<0.01 *Tagln*$^{Cre-}$ vs *Tagln*$^{Cre+}$, Mann-Whitney test. D – Representative images showing αSMA and active CASPASE-3 staining. Quantification of the number of active CASPASE-3-positive apoptotic cells in the media is shown on the right. *p<0.05 *Tagln*$^{Cre-}$ vs *Tagln*$^{Cre+}$, Mann-Whitney test. E-F – Primary VSMCs were derived from the aorta of *Tagln*$^{Cre-}$ and *Tagln*$^{Cre+}$ *Atg5*$^{flox/flox}$ mice and cultured for 4-7 passages prior to analysis. Mean ± SEM of technical quadruplicates are shown. E – Serum starved VSMCs were stimulated with serum and cell density analyzed by MTT. *p<0.05, ***p<0.001 *Tagln*$^{Cre-}$ vs *Tagln*$^{Cre+}$ at each time point, 2-way ANOVA followed by uncorrected Fisher's test. F – BrdU incorporation by serum starved VSMCs and cells supplemented with FBS for 48 hours. *p<0.05 *Tagln*$^{Cre-}$ vs *Tagln*$^{Cre+}$ with 10% FBS, Mann-Whitney test.

G – VSMCs were incubated with increasing doses of Thapsigargin for 16 hours. Cell density was analyzed using MTT assay and normalized to untreated *Tagln*$^{Cre-}$ cells. **p<0.01,

***p<0.001 *Tagln*$^{Cre-}$ vs *Tagln*$^{Cre+}$ at each time point, 2-way ANOVA followed by uncorrected Fisher's test.

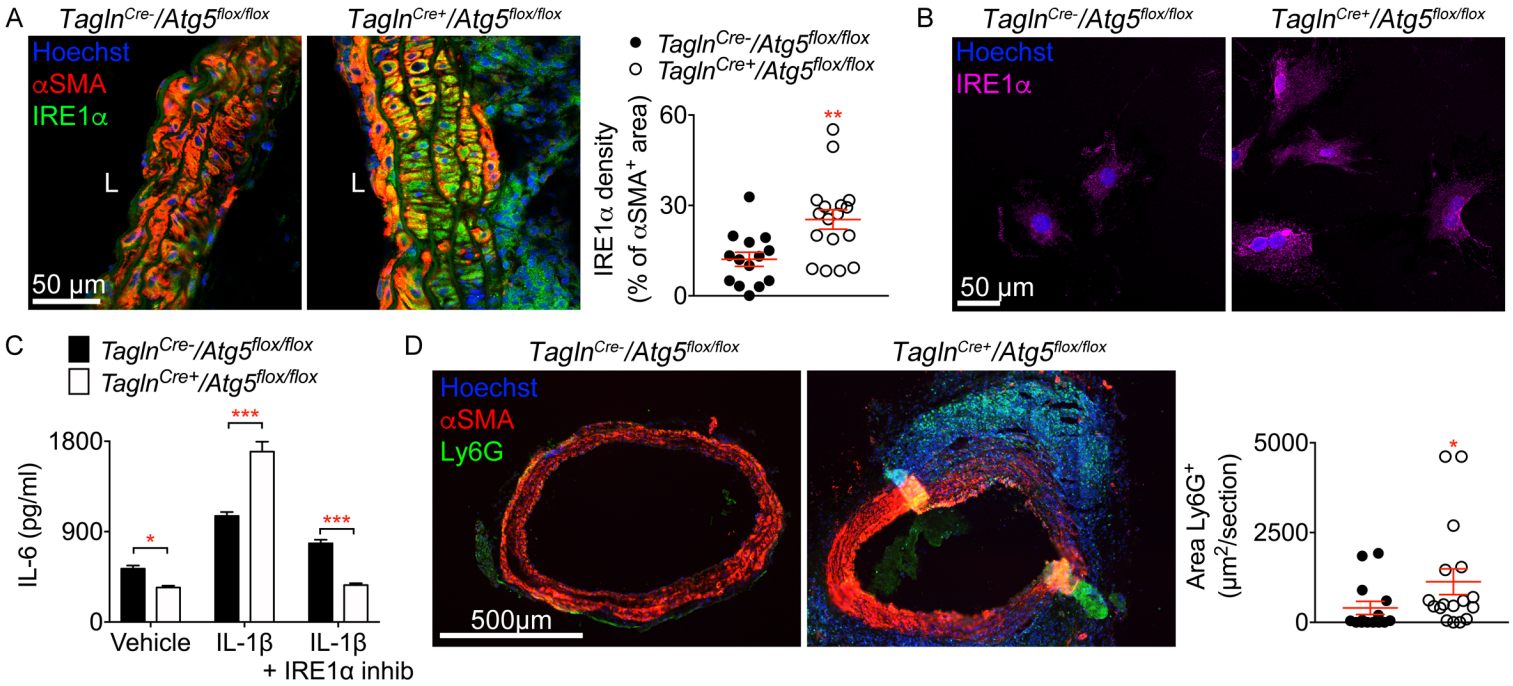

Figure 6. ATG5 deficiency in VSMCs promotes inflammation via the ER-stress sensor IRE1α.

A – Representative images and quantification of IRE1α immunofluorescence signals in αSMA$^+$ cells on aortic cross-sections from *Tagln*$^{Cre-}$ (n=14, black) and *Tagln*$^{Cre+}$ (n=17, white) *Atg5*$^{flox/flox}$ mice infused with AngII and anti-TGFβ for 28 days. **p<0.01 *Tagln*$^{Cre-}$ vs *Tagln*$^{Cre+}$, Mann-Whitney test. B – Representative images of IRE1α immunostaining of primary VSMCs derived from the aorta of *Tagln*$^{Cre-}$ and *Tagln*$^{Cre+}$ *Atg5*$^{flox/flox}$ mice cultured in vitro. C – IL-6 secretion by primary VSMCs derived from the aorta of *Tagln*$^{Cre-}$ and *Tagln*$^{Cre+}$ *Atg5*$^{flox/flox}$ mice stimulated for 16 hours with IL1β (100 pg/ml) in the presence or absence of the IRE1α kinase inhibitor (Apy29, 20μM) in vitro. Mean ± SEM of technical quadruplicates are shown. *p<0.05, ***p<0.001 *Tagln*$^{Cre-}$ vs *Tagln*$^{Cre+}$, 2-way ANOVA followed by uncorrected Fisher's test. D – Representative images and quantification of Ly6G immunostaining on aortic cross-sections from *Tagln*$^{Cre-}$ (n=14) and *Tagln*$^{Cre+}$ (n=17) *Atg5*$^{flox/flox}$ mice infused with AngII + anti-TGFβ for 28 days. *p<0.05 *Tagln*$^{Cre-}$ vs *Tagln*$^{Cre+}$, Mann-Whitney test.

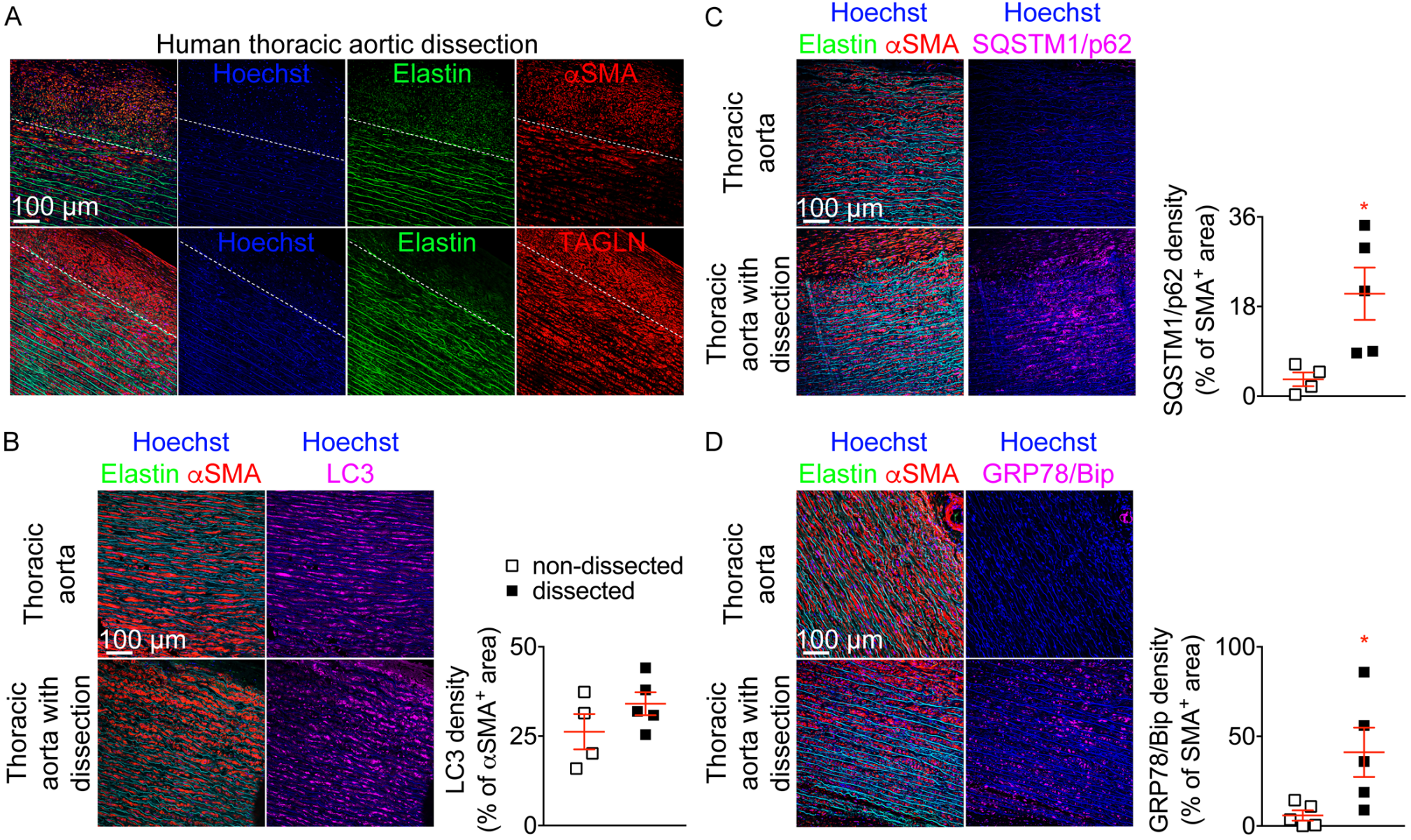
A
Human thoracic aortic dissection
Hoechst
Elastin
αSMA
100 μm
Hoechst
Elastin
TAGLN
B
Hoechst
Elastin αSMA
Hoechst
LC3
Thoracic aorta
Thoracic aorta with dissection
100 μm
non-dissected
dissected
LC3 density (% of αSMA+ area)
50
25
0
C
Hoechst
Elastin αSMA
Hoechst
SQSTM1/p62
Thoracic aorta
Thoracic aorta with dissection
100 μm
SQSTM1/p62 density (% of SMA+ area)
36
18
0
*
D
Hoechst
Elastin αSMA
Hoechst
GRP78/Bip
Thoracic aorta
Thoracic aorta with dissection
100 μm
GRP78/Bip density (% of SMA+ area)
100
50
0
*

Figure 7. Human aortic dissections are associated with impaired autophagy and ER-stress response in VSMCs.
A-D – Human thoracic aortic samples from non-dissected (n=4-5) and dissected (n=5) aortas were immunostained and analyzed by confocal microscopy. A –Representative images showing that αSMA$^+$ and TAGLN$^+$ cells are detected outside the media (dotted line depicts the external elastic laminae) in the adventitial layer of dissected thoracic aorta (4 out of 5 samples) but not in non-dissected samples (0 out of 5 samples). B-D – Representative images and quantification of the expression of LC3 (B), SQSTM1/p62 (C) and GRP78/Bip (D) in αSMA$^+$ cells in the media of non-dissected (n=4-5, white) and dissected aortic samples (n=5, black). *$p<0.05$ non-dissected vs dissected, Mann-Whitney test.

SUPPLEMENT MATERIAL

Vascular Smooth Muscle Cell Plasticity and Autophagy in Dissecting Aortic Aneurysms

Clement et al.

SUPPLEMENTAL METHODS

Animals

All the experiments were approved by the local ethics committee and done under Home Office, UK licenses PA4BDF775 and 70/7555.

In order to lineage label VSMCs, *Myh11-CreERt2/ROSA26-Confetti and Myh11-CreERt2/ROSA26-Confetti/Apoe*$^{-/-}$ male mice (previously described in Chappell et al.[1]), received 10 injections of tamoxifen diluted in corn oil (1mg/mouse/injection, i.p.) over 2 weeks. Mice were left for a week to clear excess tamoxifen, before further treatment.

Myh11-CreERt2/ROSA26-Confetti mice were infused with AngII (1µg/min/Kg, Sigma) using osmotic pumps and anti-TGFβ (10mg/Kg, clone 1.D.11, BioXCell) was injected i.p. (3 times/week) and tissues were harvested at different time points between day 7 and day 28. Out of 22 animals treated with AngII, 4 died within one week and were excluded from the analysis. Of the remaining, 6 animals showed macroscopic evidence of aortic dissection and were analyzed for VSMC phenotype by confocal microscopy. Additionally, one of the animals which appeared to have a normal aorta was also analyzed by confocal microscopy.

Myh11-CreERt2/ROSA26-Confetti/Apoe$^{-/-}$ mice were infused with AngII (1µg/min/Kg) using osmotic pumps, and inhibition of TGFβ activity (10mg/Kg, clone 1.D.11, 3 times/week, i.p.) started 14 days after the beginning of AngII infusion. Mice were injected daily with EdU (1mg/mouse) i.p. for a week, starting on day 14. A total of 25 animals were treated with AngII in three independent experiments and 10 of these received anti-TGFβ injections (5 animals per experiment in two experiments). All animals were processed for analysis by confocal microscopy.

For flow cytometry experiments, 5-month-old male *Apoe*$^{-/-}$ mice were subjected to AngII infusion (n=13), or left untreated (n=4), for 21 days later. 2 out of the 6 mice infused with AngII developed an aortic dissection. Aortic tissues were harvested,

dispersed enzymatically to a single cell suspension as described [2] and analyzed by flow cytometry.

Tagln^{Cre+} mice (Jax n°004746) and *Atg5*$^{flox/flox}$ mice (kindly provided by Noburu Mizushima, University of Tokyo) were crossed and male littermates *Tagln*$^{Cre+}$ (n=14) and *Tagln*$^{Cre-}$ (n=17) on *Atg5*$^{flox/flox}$ background were infused with AngII (1µg/min/Kg, Sigma) and anti-TGFβ (10mg/Kg, clone 1.D.11, 3 times/week, i.p.). Data are from 2 independent experiments. Blood pressure measurements were obtained by the tail cuff method. Necropsies were performed to confirm vascular rupture of animals that died prior to day 28, and the aortas were harvested and fixed in 4% PFA. Surviving mice were culled at day 28, perfused with cold PBS and aortic samples were fixed in PFA 4% overnight at 4°C, and kept in PBS at 4°C for further investigation. Assessment of aortic dissection stage (I-normal appearance; II-thickening of the aortic wall; III-dissection; IV-fatal aortic rupture) was done blinded to genotype.

Tissue processing and quantification of medial patches in lineage-traced animals. Aortas were fixed in 4% PFA overnight at 4°C, embedded in OCT and cryosectioned (12 µm) as described in Chappell et al. [1]. Sections were stained for antigens of interest, EdU incorporation and the nuclei were counter stained with DAPI as described [1] using the primary antibodies listed below, except for αSMA stainings that were done using a biotinylated primary antibody (Abcam clone 1A4) and Alexa Fluor® 647 Streptavidin (Biolegend). Secondary antibodies were all Alexa Fluor® 647 conjugated to avoid spectral overlap with the Confetti reporter proteins. Sections were mounted in RapiClear and imaged using an Sp8 Leica confocal microscope as previously described [1], with a 2.5 µm distance between scans. The number of EdU+ cells per section was quantified in Imaris (Bitplane, Oxford Instruments) to ensure that EdU+ nuclei were scored correctly for Confetti signal. Quantification of Confetti patch size within the media was performed in imaged sections within the Imaris section viewer, with Z-stack thickness of 3.5 µm. Within each "ring" of the artery (delineated by the elastic lamella) each cell was scored for its Confetti color (or absence of) cell by cell and the frequency of occurrence of contiguous runs of one Confetti color calculated for each patch size.

Immunofluorescence. Aortic samples were cleaned of surrounding tissues, embedded in OCT and cryosectioned. Immunofluorescent stainings were performed as described in Clement et al. [2]. Sections were stained with mouse anti-mouse/human αSMA-Cy3™ (Sigma, clone: 1A4), rabbit anti-mouse HMOX1 (Abcam, clone: EP1391Y), rat anti-mouse CD68 (Biorad clone: FA-11), rat anti-mouse LAMP2 (SantaCruz biotech, clone: M3/84), rabbit anti-mouse ATG16L1 (Cell Signaling Technology®, clone: D6D5), rabbit anti-mouse ATG5 (LifeSpan BioSciences LS-B1843), rabbit IgG control (Abcam ab27478), rabbit anti-mouse/human LC3 (Cell Signaling Technology®, clone: D11), rabbit ant-mouse/human Sqstm1/p62 (Abcam, ab207305), rabbit anti-mouse active CASPASE3 (Cell Signaling Technology®, clone: D3D9), rabbit anti-mouse/human IRE1α (Cell Signaling Technology®, clone: 14C10), rat anti-mouse Ly6G (eBiosciences, clone: RB6-8C5), rabbit anti-human GRP78/Bip (Cell Signaling Technology®, clone: C50B12) and rabbit anti-human TAGLN (Abcam, ab14106). Primary antibodies were revealed using donkey anti-rabbit Alexa Fluor® 555 (Invitrogen), goat anti-rat Alexa Fluor® 488 (Invitrogen) or goat anti-rabbit Alexa Fluor® 647 (Invitrogen, and Abcam ab150079).

EdU incorporation was detected using the Click-iT® Plus EdU Alexa Fluor® 647 Imaging kit (Life Tehcnologies) according to the manufacturer's instructions.

Sections from human aortic samples were obtained by P. Bruneval, Paris, France. At the time of collection, those samples were considered waste necropsy or post-surgery material and did not require specific ethics approval. Human samples from non-dissected thoracic aortas (n=5) were obtained from men (age 44-68 years old) suffering from traumatic injury of the ascending aorta (n=1), valvular surgery (n=1) or from transplantation-recused hearts (n=3). Tissues from dissected thoracic aortas (n=5; 4 ascending, 1 descending) were obtained from men (age 53-75 years old) suffering from chronic (n=3) or acute dissection (n=2) associated with degenerative disease (no bicuspid valves). Deparaffinization and staining were performed as described in Clement et al. [2]. Imaging of epifluorescent and brightfield stainings was performed using a Leica DM6000B microscope, and images were analyzed using Adobe Photoshop CS5 and ImageJ (NIH). Immunofluorescent imaging by confocal microscopy was done using a Carl Zeiss LSM 700 confocal microscope and Zen2009 software.

Perl's staining and assessment of iron accumulation. Sections were stained according to the manufacturer's instructions (Sigma, HT20-1KT). Iron staining was graded as follow: I-no iron deposition; II-mild iron deposition; III-high iron accumulation in some cells; IV-high accumulation of iron in numerous cells.

Flow cytometry. Aortic samples were digested and cell suspensions were stained following the protocol described in Clement et al. [2]. Extracellular antigens were stained using rat anti-mouse CD45-eVolve605™ (eBiosciences, clone: 30F11) or anti-CD45-APC, (Biolegend, clone: 30F11), rat anti-mouse CD31-PE-Cy7 (eBiosciences, clone: 390), rat anti-mouse CD90.2-BV786™ (BD Biosciences, clone: 53-2.1) and Zombie Yellow™ Fixable Viability Kit (Biolegend). Cells were then fixed/permeabilized using a transcription factor staining buffer set (eBioscience™ Foxp3) according to the manufacturer's instructions, and intracellular antigens were stained using mouse anti-mouse αSMA-Cy3™ (Sigma, clone: 1A4), rat anti-mouse CD68-BV605™ (Biolegend, clone: FA-11), rat anti-mouse LAMP2-FITC (eBiosciences, clone: eBioABL-93), anti-Ter-119-FITC (eBiosciences, clone: Ter-119). Flow cytometric acquisition of the cell suspension was performed on a LSR II Fortessa (BD biosciences) equipped with 4 lasers (405, 488, 561 and 640 nm). Analysis was done using BD FACSDiva Software 6.0 and figure-displayed dot plots and histograms were obtained using FlowJo software (TreeStar).

Cell culture. VSMC primary cultures were obtained using aortas from female *Atg5*$^{flox/flox}$ *Tagln*$^{Cre-}$ and *Tagln*$^{Cre+}$ littermates. Briefly, aortas were cleaned from surrounding tissues, minced into small pieces, and subjected to enzymatic digestion (RPMI 1640, collagenase D [0.2 mg/ml, Roche], dispase [1 U/ml, Stemcell™ Technologies] and elastase [1 mg/ml, Worthington biochemical Corporation]) for 45 min at 37°C. Cells were allowed to grow in complete medium (RPMI 1640 containing L-glutamine + 10 % [vol/vol] heat-inactivated FBS, 100 IU/ml penicillin, 100 µg/ml streptomycin) until passage 4 and were then aliquoted and frozen in liquid nitrogen. Serum induced proliferation of VSMC was done after overnight serum starvation (0.5% serum) and complete medium was added onto the cells. Cell density was evaluated using MTT assays (CGD1-1KT, Sigma). For DNA synthesis analysis, cells were incubated with in the same conditions, and the medium (0.5% or 10% FBS) was

supplemented with BrdU (1mM). Cells were harvested 48 hours after FBS supplementation and BrdU incorporation was analyzed by flow cytometry according the manufacturer's instruction (BD Biosciences, Kit BrdU, cat number: 559619). IL-6 production after IL-1β stimulation was performed on cells plated at $1x10^5$ cells/well, left overnight to adhere in complete medium. Cells were washed and stimulated with fresh medium containing either 0.1% DMSO (vehicle), vehicle + IL-1β (100 pg/ml, Biolegend), or IL-1β + Apy29 (20 µM, Tocris). After 24 hours, supernatants were collected and IL-6 secretion was analyzed using CBA Mouse IL-6 Flex Set (BD Biosciences). Death induced by thapsigargin (Sigma) was measured on VSMCs plated at $1x10^5$ cells/well, left overnight to adhere in complete medium. Medium was replaced with fresh medium containing increasing concentration of thapsigargin (0-1µM). After 24 hours, cell density was assessed using MTT assay. Tests were performed in quadruplicate.

Quantitative real time polymerase chain reaction. RNA was harvested from VSMCs 24 hours after plating ($1x10^5$ cells/well, in quadruplicate), extracted using RNeasy minikit (Qiagen) following manufacturer's instructions. 150 ng of RNA was reverse-transcribed (QuantiTect Rev. Transcription Kit; Qiagen) and 5 µl of cDNA (diluted 20-fold) was used to analyze the expression of *Atg5* using SYBR Green qPCR mix (Eurogentec) on a Roche lightcycler with the following primers: *Atg5* for 5'->3': CCCCTGAAATGGCATTATCCAA; *Atg5* rev 5'->3': AAAGTGAGCCTCAACCGCAT.
Il6 for 5'->3': CCAGAGATACAAAGAAATGATGG; *Il6* rev 5'->3': ACTCCAGAAGACCAGAGGAAAT. *Cxcl1* for 5'->3': CAGACCATGGCTGGGATTCA; *Cxcl1* rev 5'->3': AGTGTGGCTATGACTTCGGTTT. *Ccl2* for 5'->3': GTTAACGCCCCACTCACCT; *Ccl2* rev 5'->3': TTCTTTGGGACACCTGCTG. House keeping gene: *36b4* for 5'->3': TCTCCAGAGGCACCATTGAAA; *36b4* rev 5'->3' CTCGCTGGCTCCCACCTT.

Statistical analysis. Values are shown as average ± SEM. Statistical analysis was performed using Prism GraphPad and differences between groups were evaluated using Mann-Whitney test (2 groups), Kruskal-Wallis test followed by uncorrected Dunn's test (> 2 groups), 2-way ANOVA (cell proliferation/survival) or Chi-squared

test (Distribution between 2 groups), as indicated in the figure legends. Results were considered statistically different at $p<0.05$.

SUPPLEMENTAL FIGURES and FIGURE LEGENDS

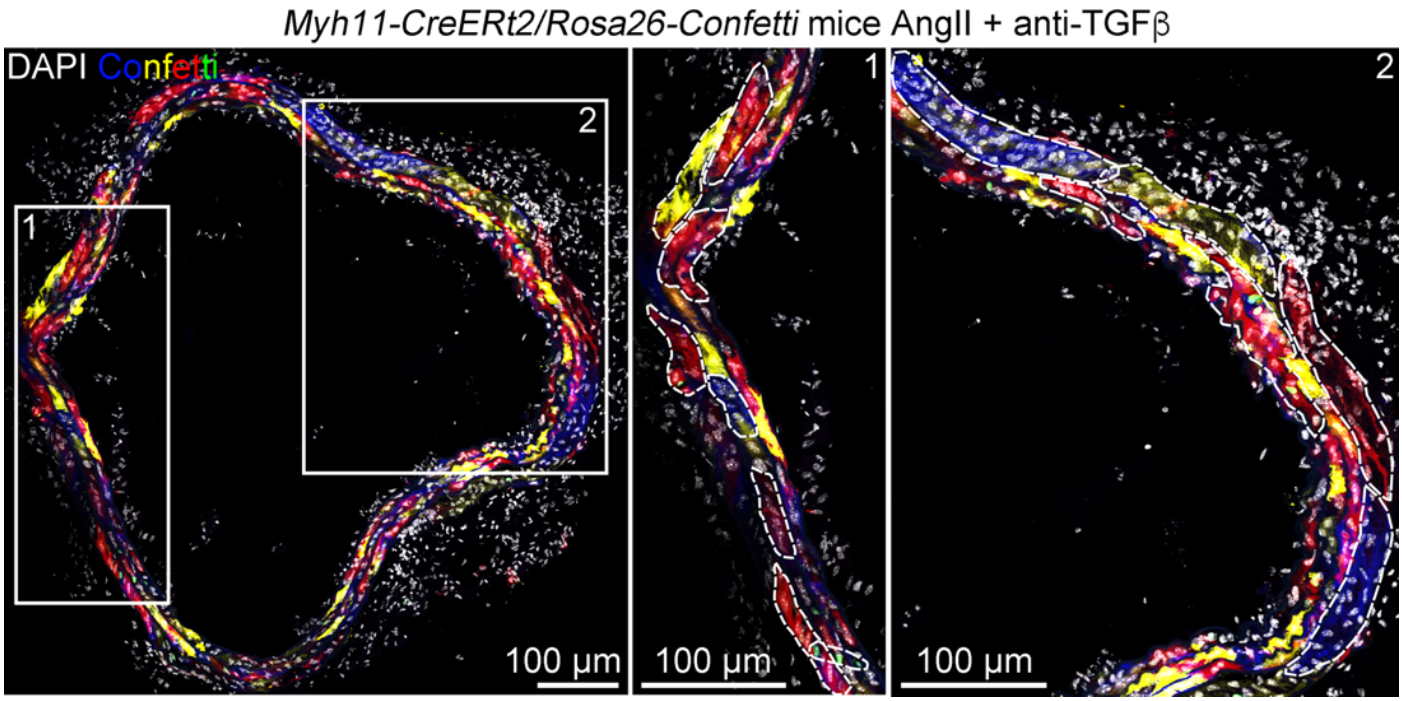

Figure I: Monochromatic patches in the media of *Myh11-CreERt2/Rosa26-Confetti* mice after AngII + anti-TGFβ infusion.
Representative pictures of monochromatic patches of VSMCs in the media of *Myh11-CreERt2/Rosa26-Confetti* mice after AngII + anti-TGFβ infusion analyzed by confocal microscopy. In the insets, dashed lines are circling monoclonal patches.

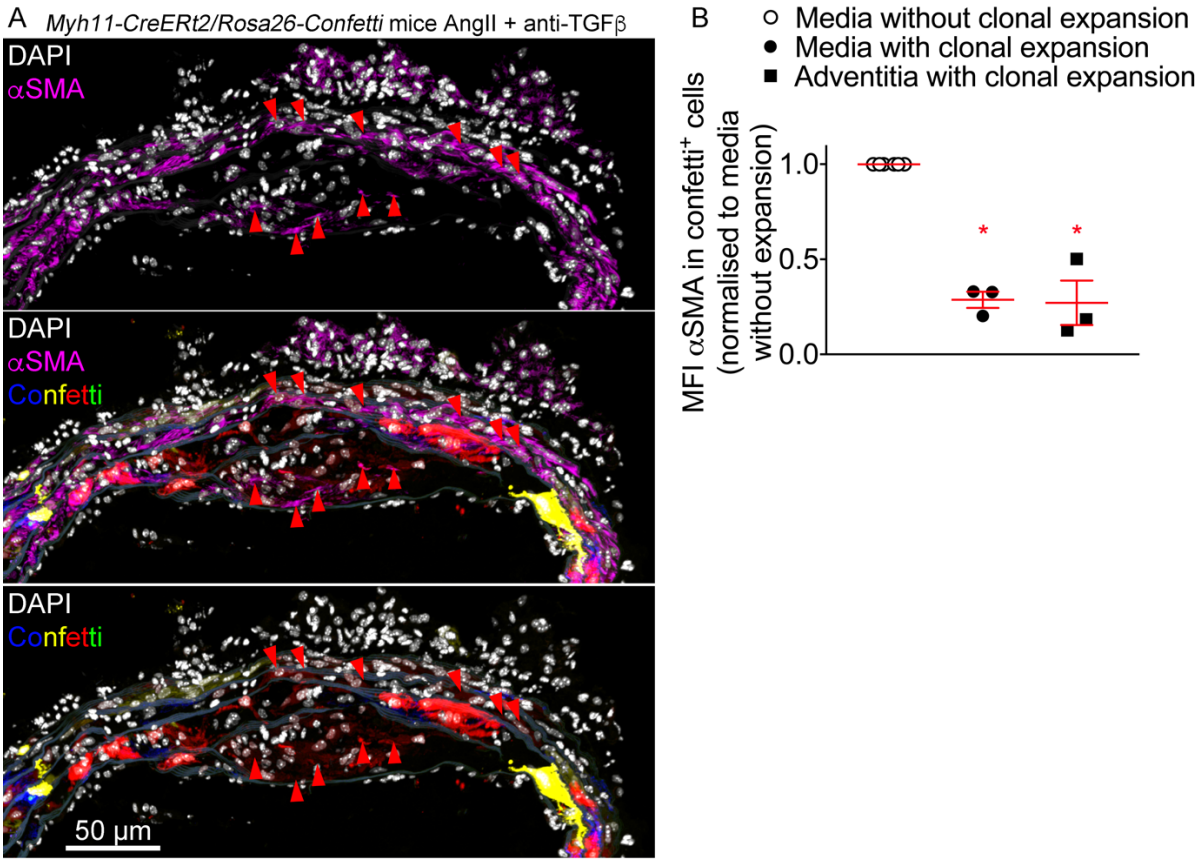

Figure II: Reduced expression of αSMA by clonally expanded medial VSMCs.
A – Representative images of αSMA staining of aortic cross sections from *Myh11-CreERt2/Rosa26-Confetti* mice after AngII + anti-TGFβ infusion. Monochromatic patches express lower levels of αSMA, compared to regions displaying the mosaic color pattern also observed in healthy vessels. Red arrow heads point to αSMA^+ Confetti-positive cells in a red patch of clonally expanded VSMCs.
B – Quantification of αSMA mean fluorescence intensity (MFI) in $Confetti^+$ cells from areas of the media, without clonal expansion (white circles) versus medial monochromatic patches (black circles, n=3) or adventitial outgrowths (black squares, n=3). For each region, 15 cells were analyzed per animal, and the MFI of αSMA from the expanded cells was normalized to the MFI of non-expanded cells from the same section (white circles). A total of 6 animals were used for quantification. *$p<0.05$ in media without clonal expansion vs other conditions. Kruskal-Wallis test followed by uncorrected Dunn's test.

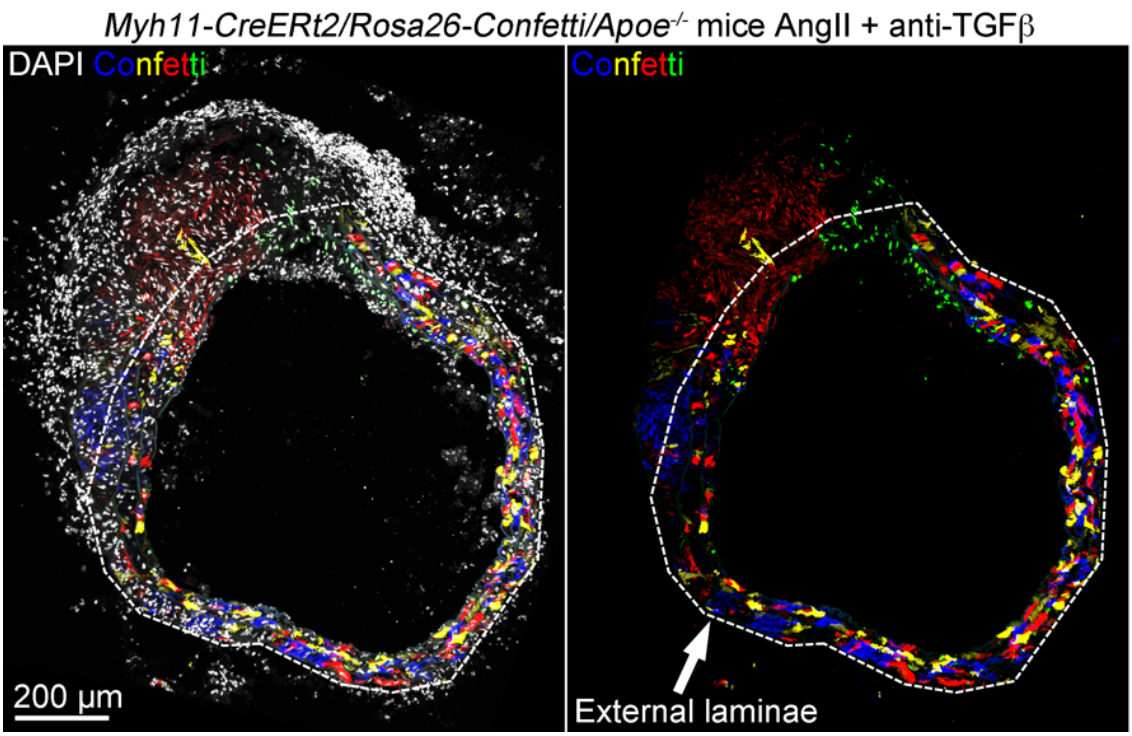

Figure III: Blocking TGFβ activity does not impair VSMCs outgrowth after aortic dissection.
Representative images showing clonally expanded VSMCs in the adventitia of a *Myh11-CreERt2/Rosa26-Confetti/Apoe*$^{-/-}$ animal that developed dissection after 28 days of AngII infusion and inhibition of TGFβ activity at day 14. The external elastic laminae is outlined.

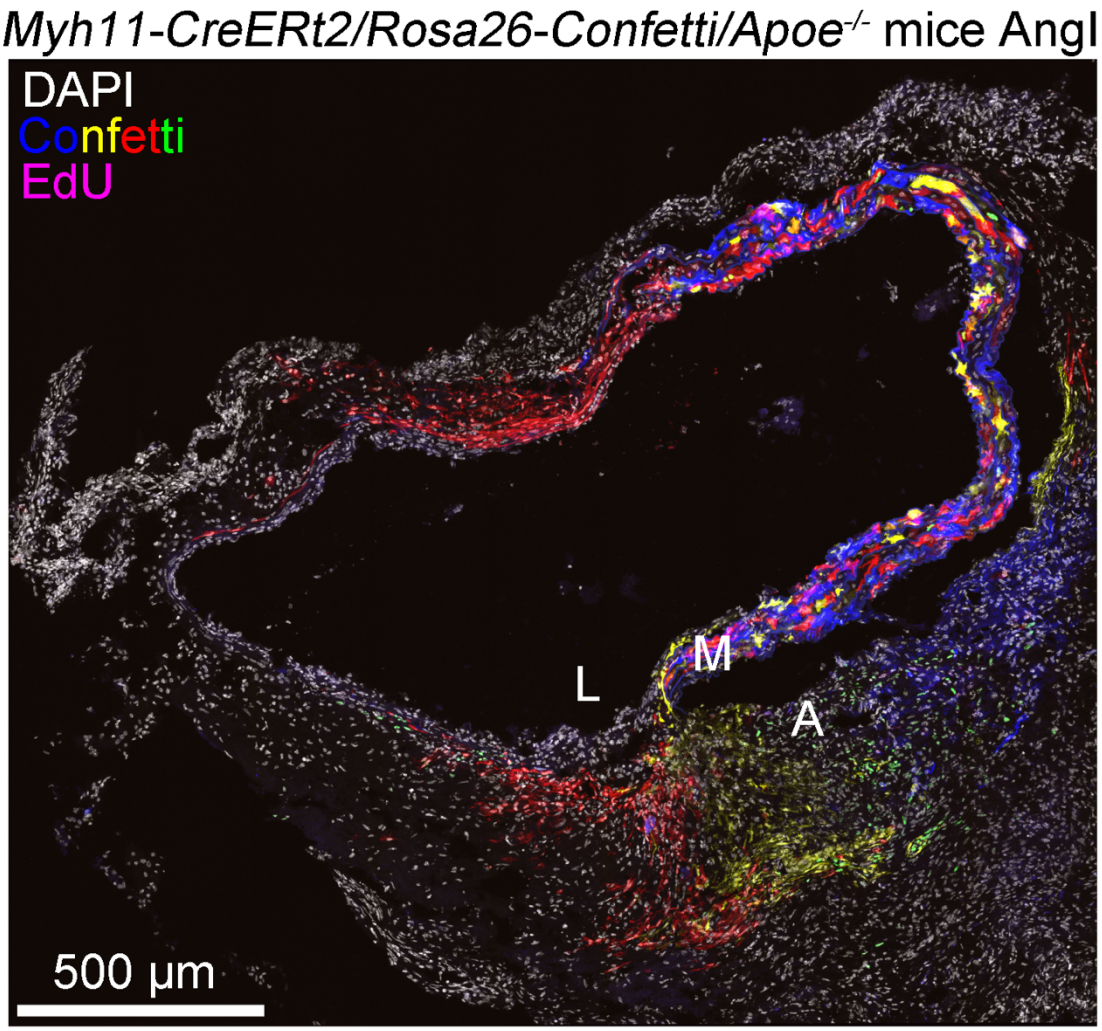

Figure IV: Representative image at low magnification of Figure 3F.
L: Lumen, M: Media, A: Adventitia.

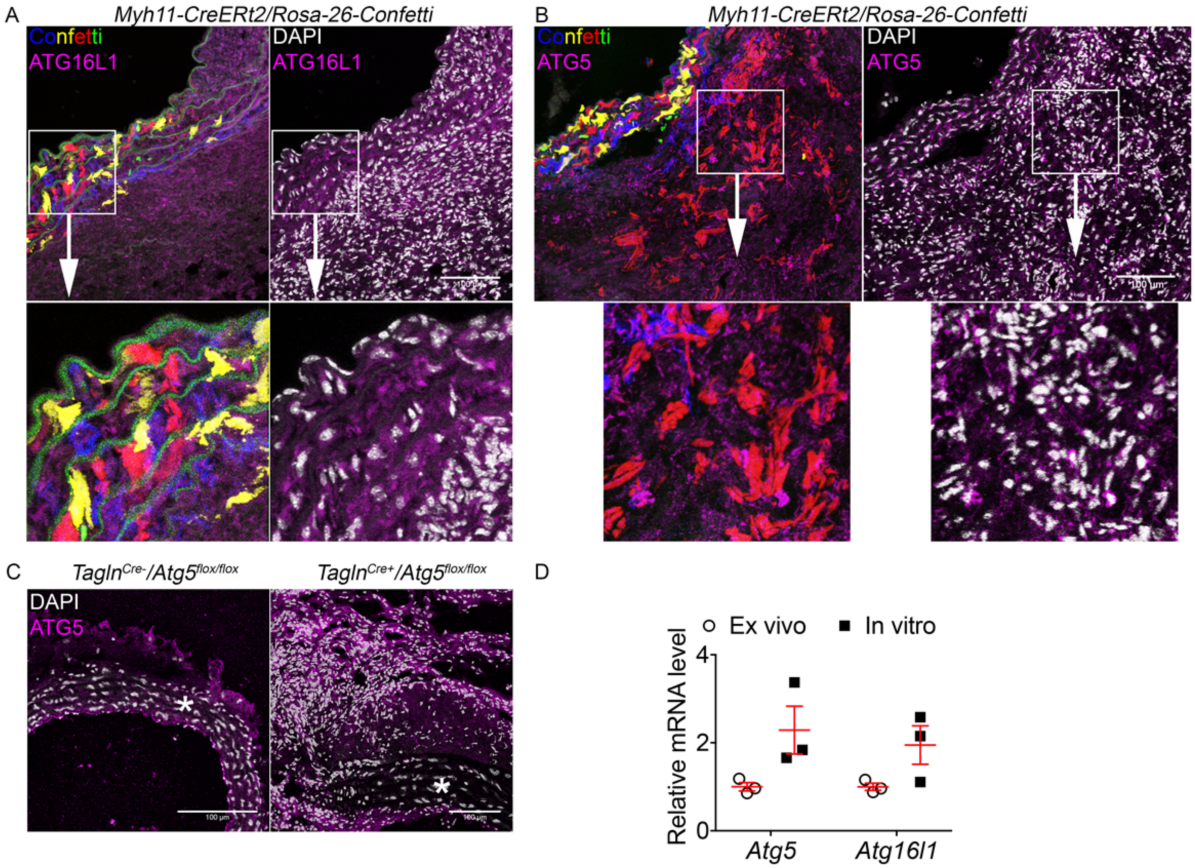

Figure V. Expression of autophagy related genes in phenotypically switched VSMCs.

A-C – Representative images of ATG16L1 (A) and ATG5 (B, C) staining (magenta) of aortic cross sections from AngII-treated, VSMC lineage labelled (*Myh11-CreERt2/Rosa26-Confetti)* mice with aortic dissection (A, B) and *Tagln*$^{Cre-}$, *Atg5*$^{flox/flox}$ and *Tagln*$^{Cre+}$, *Atg5*$^{flox/flox}$ mice (C).

D – Analysis of *Atg5* and *Atg16l1* expression by RT-Q-PCR in *ex vivo* and primary VSMCs cultured at passage 4. Mean ± SEM of biological triplicates, normalized to house keeping genes (*Yhwaz* and *Hprt*) are shown.

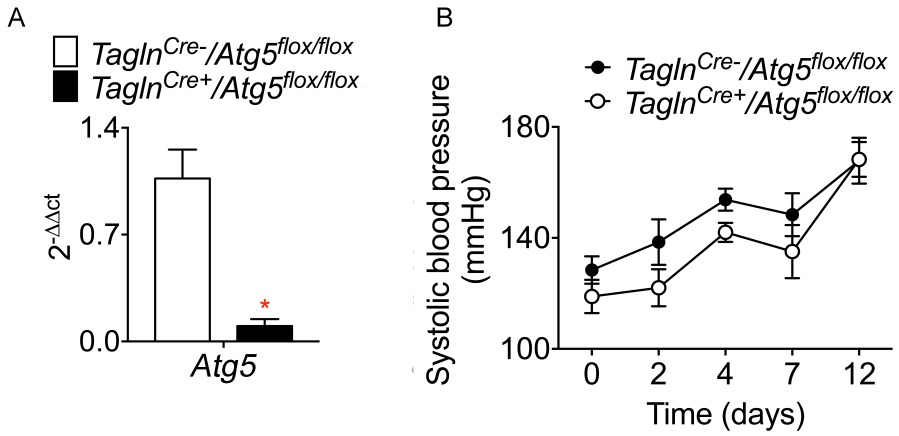

Figure VI. Expression of *Atg5* and blood pressure measurements in *Tagln*$^{Cre-}$ and *Tagln*$^{Cre+}$ *Atg5*$^{flox/flox}$ mice.

A – Analysis of *Atg5* expression by RT-Q-PCR of primary VSMCs derived from the aortas of *Tagln*$^{Cre-}$ and *Tagln*$^{Cre+}$ *Atg5*$^{flox/flox}$ mice. *p<0.05 *Tagln*$^{Cre-}$ vs *Tagln*$^{Cre+}$, Mann-Whitney test. Data were obtained using technical quadruplicates and are representative of two independent experiments.

B – Systolic blood pressure (mmHg) from *Tagln*$^{Cre-}$ (black, n=14 at the beginning of the experiment) and *Tagln*$^{Cre+}$ (white, n=17 at the beginning of the experiment) *Atg5*$^{flox/flox}$ mice before (day 0) and following AngII + anti-TGFβ infusion.

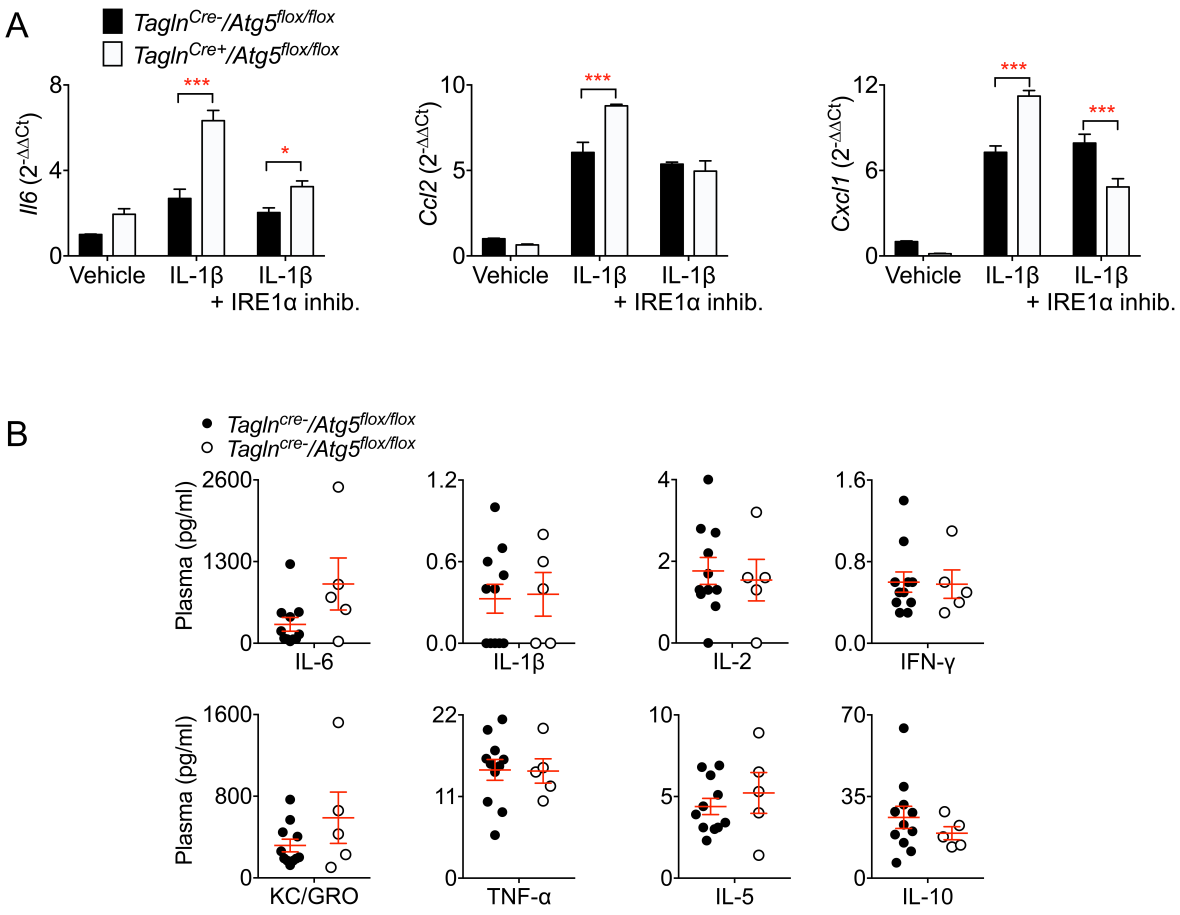

Figure VII. Atg5 deficiency in SMCs promotes a pro-inflammatory phenotype via IRE1α.

A- Analysis of *Il6*, *Ccl2* and *Cxcl1* expression by RT-Q-PCR of primary VSMCs derived from the aortas of *Tagln*$^{Cre-+}$ *Atg5*$^{flox/flox}$ and *Tagln*$^{Cre+}$ *Atg5*$^{flox/flox}$ mice stimulated for 16 hours with IL1β (1 µg/ml) in the presence or absence of the IRE1α kinase inhibitor (Apy29, 20µM) in vitro. Mean ± SEM of technical quadruplicates are shown. *p<0.05, ***p<0.001 *Tagln*$^{Cre-}$ vs *Tagln*$^{Cre+}$, 2-way ANOVA followed by uncorrected Fisher's test.

B- Analysis of circulating cytokines (IL-6, IL-1b, IL-2, IFNg, KC/GRO, TNFa, IL-5, IL-10) in the plasma of surviving *Tagln*$^{Cre-}$ *Atg5*$^{flox/flox}$ (n= 11) and *Tagln*$^{Cre+}$ *Atg5*$^{flox/flox}$ (n=5) mice infused with angiotensin II and anti-TGFβ at day 28.

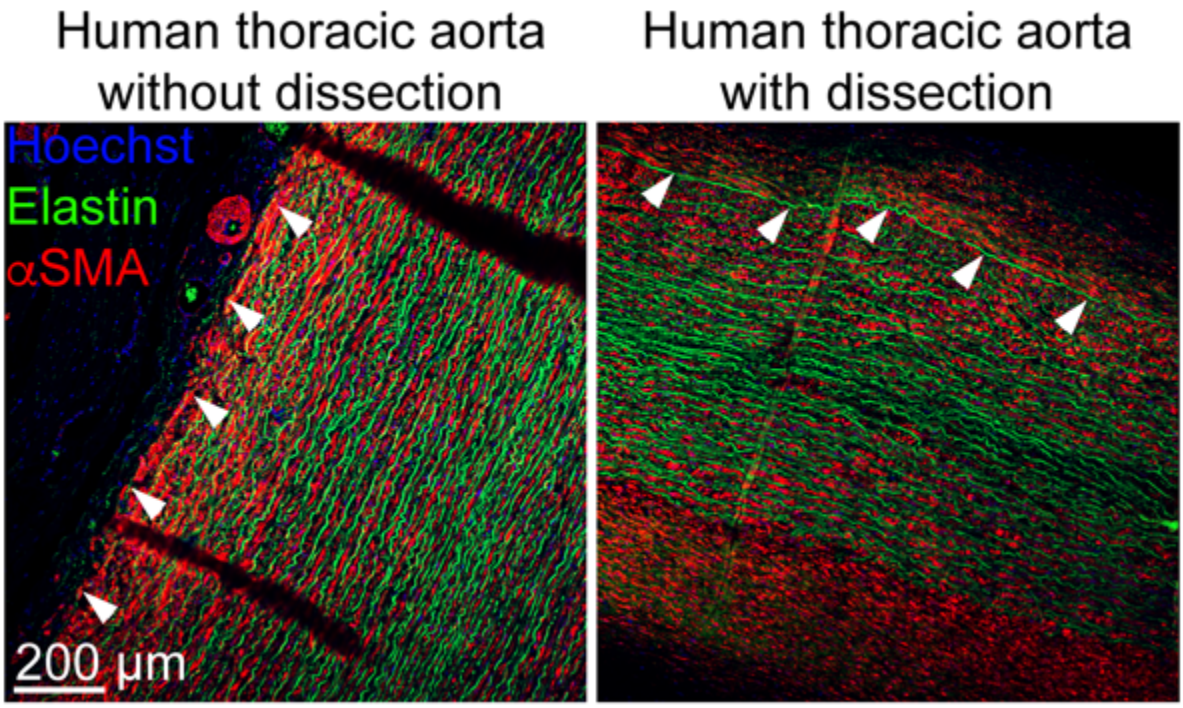

Figure VIII. αSMA expression in human thoracic aorta.
Representative images of αSMA staining on human thoracic aorta without dissection (n=5) or with dissection (n=5) showing αSMA^{+} cells in the adventitia of dissected aorta (arrow head showing the edge of the medial layer).

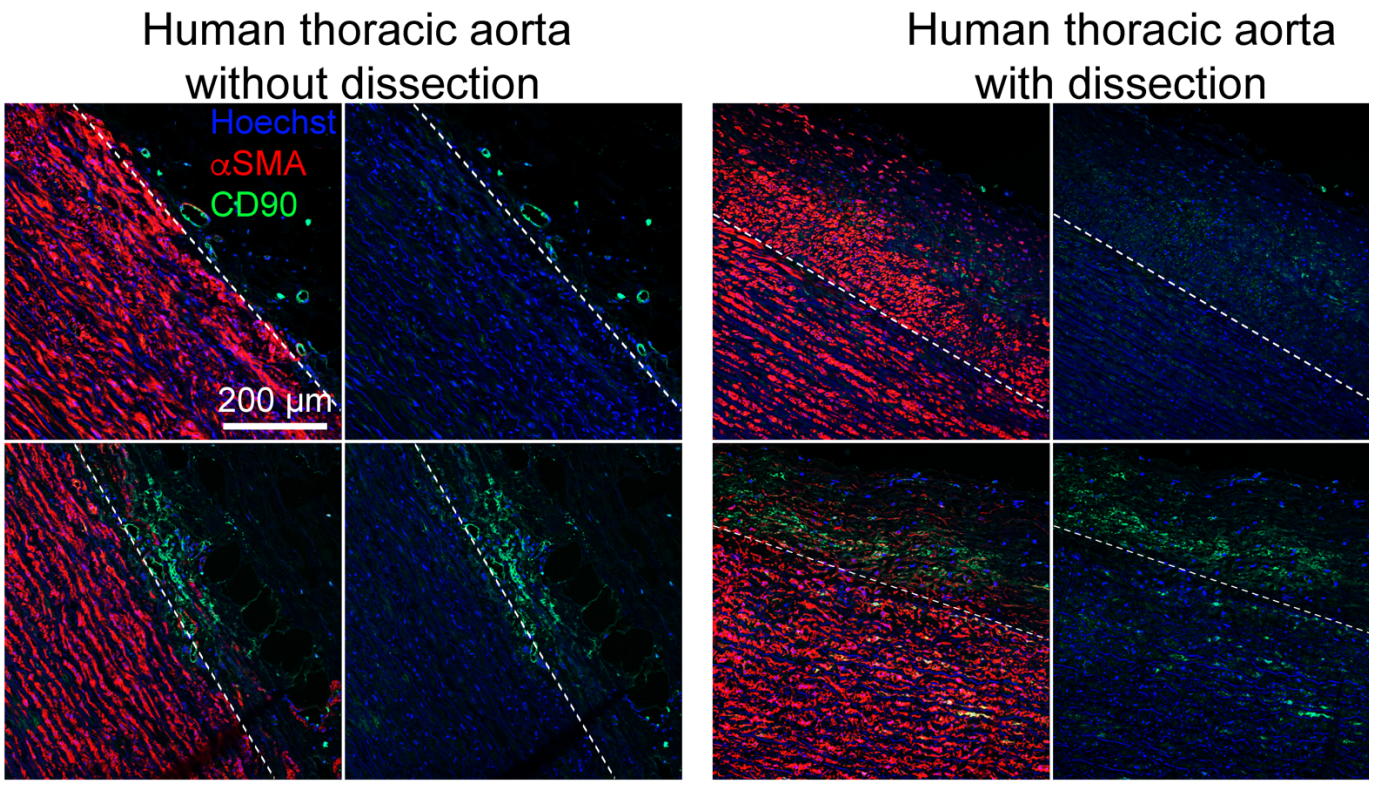

Figure IX. CD90$^-$αSMA$^+$ Human SMCs accumulate to the adventitia after aortic dissection.
Representative examples of human thoracic aorta without dissections (2 examples are shown, 4 were analyzed) and with dissections (2 examples are shown, 5 were analyzed). Most of the αSMA$^+$ cells outside of the media (limit shown by the dashed line) are CD90$^-$.

SUPPLEMENTAL REFERENCES

1. Chappell J, Harman JL, Narasimhan VM, Yu H, Foote K, Simons BD, Bennett MR, Jorgensen HF. Extensive Proliferation of a Subset of Differentiated, yet Plastic, Medial Vascular Smooth Muscle Cells Contributes to Neointimal Formation in Mouse Injury and Atherosclerosis Models. *Circ Res*. 2016;119:1313-1323.

2. Clement M, Haddad Y, Raffort J, Lareyre F, Newland SA, Master L, Harrison J, Ozsvar-Kozma M, Bruneval P, Binder CJ, Taleb S, Mallat Z. Deletion of IRF8 (Interferon Regulatory Factor 8)-Dependent Dendritic Cells Abrogates Proatherogenic Adaptive Immunity. *Circ Res*. 2018;122:813-820.